A Novel Approach for Optimal Deployment of Plug-in Electric Vehicles with Integrated Renewable Energy Sources

Jamiu O. Oladigbolu[1], Mohd Bilal[2], Saket Gupta[3], Asad Mujeeb[4] and Li Li[5]

[1]Department of Electrical and Computer Engineering, Faculty of Engineering, King Abdulaziz University, Jeddah 21589, Saudi Arabia.
[2]Electrical Engineering, SND College of Engineering and Research Center, Yeola, Nashik, Maharashtra, 423401, India
[3]Department of Instrumentation and Control Engineering, Bharati Vidyapeeth College of Engineering, Delhi-110063, India
[4]Department of Electrical Engineering, Tsinghua University, Beijing, 100084, China.
[5]School of Electrical and Data Engineering, University of Technology Sydney, Sydney, NSW 2007, Australia

Correspondence should be addressed to Mohd Bilal: bilal.zhcet01@gmail.com

Abstract:

The electrification of transportation significantly impacts the dynamics of distribution networks (DNs), necessitating a strategic approach to deploying plug-in electric vehicle charging stations (PEVCSs). This study introduces a pragmatic methodology for determining optimal locations for PEVCSs within the IEEE 33-bus system framework. The motivation behind this research stems from the need to enhance DN reliability and efficiency while accommodating the growing demand for electric vehicle charging, thereby supporting environmental sustainability goals. The proposed model considers four principal factors: active power loss, reactive power loss, voltage regulation, and the voltage stability index (VSI). To mitigate the increased energy demand from PEVCSs, the study advocates incorporating solar-powered distributed generation (SPDG) units. A significant contribution of this research is the introduction of two-loss sensitivity factors (LSFs) designed to rank load buses by their criticality, ensuring a more targeted and effective deployment of PEVCSs. The model evaluates the DN's reliability post-implementation of PEVCSs and SPDGs through seven distinct case studies, ranging from baseline scenarios to individually and concurrently allocating multiple PEVCSs and SPDG units. The key findings reveal that the optimal placement of PEVCSs and SPDGs significantly decreases active power loss, reducing it from 202.67 kW in the baseline scenario to 24.59 kW in the best-case scenario. Similarly, reactive power loss is also reduced, dropping from 135.4 kVAR in the base case to 17.74 kVAR in the best-case scenario (CS 6). Additionally, integrating SPDG units improves voltage profiles and stability across the network. This model's adaptability to various geographic and climatic conditions enhances its practical utility, offering valuable insights for policymakers and industry stakeholders. The results provide a robust framework for the large-scale deployment of PEV infrastructure powered by renewable energy sources, contributing to the development of sustainable and resilient power distribution systems.

Keywords: Active power loss, Charging station, Plug-in electric vehicle, Reliability, Solar-powered distributed generation, Voltage stability index

1. Introduction

In the quest to fortify power systems (PSs) and reduce carbon emissions, smart grid development has become a focal point of research. Smart grids address multifaceted challenges, encompassing transmission, energy efficiency, and the sustainability of energy production. A critical aspect of this evolution is the strategic allocation of distributed energy resources (DER) within the electric network, which is integral to the efficacy of smart grids. DER integration bolsters grid reliability by alleviating system stress and enhancing voltage regulation [1]. A key component in this paradigm is the adoption of solar photovoltaic-based distributed generation (SPDG) units. These units are instrumental in diminishing carbon emissions from electricity generation. However, the inherent intermittency and volatility of solar

energy pose risks of grid instability. This underscores the need for advanced optimization methodologies to determine the most effective locations and capacities for SPDG unit deployment within feasible timeframes. Concurrently, plug-in electric vehicles (PEVs) are emerging as a significant facet of smart grids, lauded for their environmental sustainability. PEVs intersect the realms of transportation and energy, offering grid electricity supply capabilities. Yet, their integration is not without challenges; uncoordinated charging practices can exacerbate peak demand, posing risks to standard grid operations [2]. This has spurred research into coordinated PEV charging strategies, aiming to balance the load via peak shaving and valley filling. Another research dimension explores the optimal placement of PEV charging stations (PEVCS), focusing on performance indicators like power loss and voltage profiles within the electrical PS.

This research work presents a comprehensive model for the allocation of SPDG units and PEVCS in distribution networks (DNs), contributing to the dynamic landscape of intelligent grid development [3]. Extensive research on the siting and sizing of distributed generators (DGs) has been conducted, with various studies employing both quantitative and heuristic approaches for active power loss minimization in integrated DG allocations [4, 5]. Techniques ranging from genetic algorithms (GA) [6] to particle swarm optimization (PSO) [7], Grey wolf optimization (GWO), hybrid GWOPSO [8], bald eagle search algorithm (BESA) [9], imperialist competitive algorithm [10], multi-objective PSO (MOPSO) [11] and teaching learning based optimization (TLBO) [12], among others, have been proposed for optimum DG placement. These methodologies aim to enhance system performance and maximize profits, primarily focusing on improving voltage regulation. Additionally, optimization techniques like the harmony search algorithm are employed to optimize DG placement, aiming to minimize system losses and improve voltage levels [13]. Other studies have explored different optimization strategies, including modified differential evolution for energy loss minimization and voltage profile improvement [14]. In ref [15], a GA-based strategy has been utilized for DG optimal placement, while environmental factors were considered [14] along with technical, financial, and multi-faceted approaches considering other key essential factors. The Grasshopper optimization algorithm (GOA) has also been proposed for optimal network reconfiguration, focusing on investment cost reduction and active power loss minimization [16].

The advent of PEVs and the accompanying need for long-distance travel capabilities have necessitated the expansion of PEV charging infrastructures. These stations are pivotal in providing substantial electrical power to PEVs. With the escalating adoption of PEVs globally, a surge in the demand for charging stations across various nations is anticipated in the forthcoming years. Consequently, exhaustive research efforts are being channeled into diverse domains such as planning, design, and utilization of PEV charging facilities [17]. A two-phase optimization method for the ideal placement of PEVCSs is introduced in [18]. This method first determines optimal locations based on environmental considerations and the service radius of each station. Subsequently, the second phase involves scheduling the capacity of these stations to minimize overhead costs, encompassing investment, maintenance, usage, and loss expenses. The challenge of smart parking location in the context of electric vehicle integration is addressed in [19], focusing on maximizing benefits. A thorough survey on optimal PEV charging station allocation, considering both transportation and power networks under technical constraints, is presented in [20]. This framework incorporates a variety of technical, financial, and network security considerations. Further research, as detailed in [21], explores a multi-objective method for estimating the number and capacity of PEV parking lots and the energy scheduling of power supply resources. A quantitative model for PEV charging station placement within power networks is discussed in [22], emphasizing cost function optimization and voltage profile management. This study accounts for normalized values of objective functions to ensure precise results, subject to constraints like the number of charging stations, power balance, transmission flow, and voltage limits at each grid node.

Innovative techniques have been developed for optimal PEV charging station siting. Mixed-integer non-linear programming methods, aimed at minimizing energy loss costs, enhancing voltage profiles, and improving network reliability, are established in [23]. An analytical approach for siting and sizing PEV charging stations is proposed in [24], while a hybrid of Tabu search and PSO is utilized for optimum placement in [25]. The work in [26] devises a novel methodology for adjusting charging prices based on EV users' travel behaviors to optimize power system voltage regulation. Algorithmic and GA-based strategies for optimal vehicle flow in networks, crucial for effective charging infrastructure management, are developed in [27]. The article examines the involvement of adaptable green energy hubs which include wind power plants, biological waste units, and hydrogen, thermal, and compressed air storage facilities in the electricity market using the market clearing pricing concept. Hubs are prevalent in both electric and thermal systems. The biological waste unit is fitted with a combination of power and heat technology, which generates both electrical and thermal (ET) energy. The layout suggested takes the form of bi-level optimization. Its upper level determines how to maximize the hub's predicted profit while taking into account the operational restrictions of the

aforementioned resources and storage equipment, as well as the hub's flexibility. The market clearing pricing method is incorporated at the lower formulation level, to lower the predicted operating cost of electrical power and thermal power-producing units while adhering to the optimum power flow (OPF) equations of ET networks [28]. A two-stage optimization mechanism for coordinated scheduling of TSO-DSO energy and Ancillary services (AS) markets in the presence of renewable generators, electric vehicles, and DR aggregators is presented in [29]. The implications of PEVCS allocation on the reliability of electrical networks are elucidated in [30]. A case study conducted in South Delhi, India, as mentioned in [31], focuses on installing PEV charging stations, taking into account investment costs, PEV loss costs, connection expenses, and travel time. Here, grey wolf optimization is employed to optimize these objectives, with results compared to those obtained using PSO. Additionally, Ref. [32] proposes a GA and PSO-based strategy for determining optimal locations and EV penetration levels. Lastly, authors in [33] introduce a GA-based methodology for optimal EV charging station sizing, further contributing to the evolving landscape of PEV infrastructure development. In [34], the author examined the energy management of grid-dependent versatile energy hubs. The architecture incorporates electrical and heating (EH) networks that combine renewables and battery storage units through the hub, which acts as an interface. The objective is to reduce the predicted operating expenses of the aforementioned networks, considering the networks' ideal power flow model and the theoretical description of flexible energy hubs. The problem formulation also took into account ambiguities about the amount of demand, the cost of EH energy, and renewable power. Similarly, the industrial energy hubs with both electrical and heating networks including hydrogen demands are studied with the key objective to utilize and investigate the potential of large industrial energy hubs in the resilience improvement of PSs [35].

In [36], researchers present a holistic approach to the integration of solar-based EV Charging Stations (EVCS) into DNs. This method focuses on enhancing the voltage profile, reducing power loss, and curtailing costs. They employ a probabilistic technique to predict PEV load requirements and use a feed-forward neural network to assess solar-power generation from associated plants. Moreover, [37] explores diverse charging strategies and their effects on daily peak loads. The incremental investments required for varying degrees of PEV penetration, along with the associated energy losses and their implications, are calculated in [38]. Complementing this, Ref. [39] scrutinizes the impact of electric vehicles on DN reliability, particularly concerning voltage levels and power losses. Similarly, Ref. [40] investigates how electric motor vehicles affect grid reliability, exploring strategies to mitigate any adverse impacts. These studies predominantly concentrate on the placement and capacity of PEVCSs independent of DG units. However, the interaction between PEVs, energy storage systems (ESSs), and renewable-powered DGs in distributed energy environments has garnered significant attention. The investigation [41] uses energy storage made from compressed air to fill the gap between the patterns of power production and usage, to improve the utilization of energy and lower planning costs. In [42], a GA-based bi-level optimization model is developed for allocating wind turbine units and battery ESSs (BESSs) with ancillary regulations in an electric grid network. A novel GA-based method for optimal PEV integration in microgrids, considering uncertainties in solar-power production, energy cost, and load requirement, is proposed in [43]. Further, the authors in [44] propose a multi-objective optimization (MOO) for the location and sizing of renewable DG units and charging stations. In [45], a GOA is utilized to optimize the sizing of independent microgrid systems. A multi-stage mechanism is introduced in [46] to unlock the flexibility potential of different resources within renewable-based microgrids (RBMGs) such as IoTs-enabled smart homes (IESHs), PEVs etc. Community-based grid reinforcement processes, coordinating rooftop photovoltaics (PVs) and BESSs, are suggested in [47]. Stochastic electric vehicle charging load models, correlating with PV power supply to enhance power quality, are introduced in [48]. The combined placement of DGs and PEV parking lots in radial DNs is explored in [49], aiming to reduce losses and maintain system reliability. Researchers in [50, 51] investigated demand response programs (DRPs) and integrated demand response programs (IDRPs) through an energy management coordinated framework for the multi-energy sector including residential, industrial, and commercial energy hubs as well as to efficiently enhance the flexibility of local energy systems. In [52], the authors discussed the versatile electricity management of a network microgrid using energy from RESs and flexibility sources. These sources incorporate an innovative architecture for the interconnected unit of ESS with PEV parking and an incentive-based DRP. The suggested approach for energy management is written as an optimization challenge that seeks to reduce the disparity between the estimated energy expenditure and the anticipated profit of flexibility sources while adhering to the AC OPF, RESs, flexibility sources, and microgrid flexibility constraints.

A technique for concurrently determining the location and capacity of renewable energy sources (RESs) and PEVCSs, in addition to managing vehicle charging in the network, is introduced in [53]. This involves a multi-objective function aimed at minimizing power losses, voltage fluctuations, energy procurement costs, and vehicle battery maintenance expenses. The study in [54] focuses on locating fast charging stations in the East Delta Network, considering power losses and investment costs. The replacement of gasoline cars with PEVs and its positive influence on system

reliability is demonstrated in [55]. The role of renewable-based DGs, including photovoltaic, wind energy, micro-turbines, and fuel cells, along with various energy storage devices like batteries and flywheels, is highlighted in [56]. These technologies transform electrical power into optimal electric energy for use in electricity networks or by consumers, reducing the need for expensive generating units. The comparison of the present work with other recent research studies is tabulated in Table 1.

Table 1. Comparison of the present work with other recent research studies for the optimal deployment of PEVs with integrated SPDG units in distribution network

System for validation	Year	Objective Function	Constraints	Optimization Technique Used	Shortcomings	References
IEEE 33 bus system	2021	minimization of Energy loss, voltage deviation index (VDI), and investment cost	Power balance, voltage limit, branch thermal limit, DG penetration limit	Hybrid of Harris Hawks Optimization and GWO	The study does not account for the effects of integrating PEVs and SPDG on system reliability.	[57]
IEEE 9, 33 and 66 bus system	2020	Reliability enhancement cost, power loss improvement cost, and investment cost	Bus voltage constraint, Transmission line constraint, Parking lot capacity constraint and load flow constraint	Competition over resource algorithm	The study focuses solely on the allocation of PEVCSs, without considering the impact of PEV placement on the system's stability.	[58]
East Delta Network (30 bus system)	2024	Build up cost, Active and Reactive power loss reduction	Node voltage constraint, Active and Reactive power limit, Power balanced constraint and Number of PEV charging station constraint	Adaptive Particle Swarm Optimization	The research does not account for the unpredictable patterns and PEV usage and charging behavior, which could significantly impact the modeling and effectiveness of PEV charging stations.	[54]
Modified IEEE 34 bus system	2024	Minimizing active energy losses	Voltage limit at buses, Line current limit, Power injected by DG, Maximum DG penetration, PEVCS capacity	Genetic Algorithm	The study does not examine the impact of integrating PEVs and SPDGs on the voltage profile and voltage stability index (VSI), nor does it assess the overall system reliability.	[59]
IEEE 33 and 69 bus system	2023	Minimization of active and reactive power losses, VDI	Power requirement, Node voltage constraints, Limits on voltage angles, PV power constraints, Current constraints and Line loading constraints	Hybrid GA and PSO	The study does not investigate the stability and reliability of the DN following the integration of PEVs and SPDGs.	[60]
Indian 28 bus system	2022	Minimization of active and enhance voltage profile	Power balance constraints, Bus voltage profile	Political Optimization Algorithm	The study lacks a comprehensive analysis of the long-term operational impacts and maintenance costs	[61]

			constraints and Battery storage constraint		associated with the optimal allocation of SPDG and PEVs.	
IEEE 118 bus system	2022	Minimization of active power loss costs, voltage deviations, EV energy consumption costs, and SPDG costs	Number of PEV charging station	Hybrid GWO and PSO	The research does not adequately address the potential grid stability issues and real-time demand fluctuations caused by fast charging stations in an integrated electric transportation system.	[62]
IEEE 33 bus system	2022	Minimization of active power loss and improving voltage profile	Power balancing restrictions, Voltage restriction and Current flow restriction	Symbiotic Organism Search algorithm	The study fails to incorporate the unpredictable usage patterns of PEVs and the variability SPDG, both of which are crucial for accurately modeling and optimizing the performance of PEV charging stations.	[63]
IEEE 33 bus system	2018	Voltage stability, Reliability, and Power loss	Number of PEV charging station, Power requirement constraints, Node voltage constraints,	Genetic algorithm	The study does not consider the integration of SPDG units. Furthermore, it fails to account for the probabilistic behavior of PEVs and the intermittency of solar irradiance.	[64]
IEEE 33 bus system	2024	Minimization of active and reactive power losses, Improvement of voltage profile and VSI and Evaluation of reliability indices		Artificial Hummingbird Algorithm	This paper models the system by considering the probabilistic nature of PEVs and SPDG units, focusing on minimizing active and reactive power losses, enhancing the voltage profile, and improving system stability, while also evaluating the impact of PEV loads and SPDG units on the operational parameters of the DN in terms of reliability measures.	This paper

Reflecting on the existing literature, it becomes evident that many studies have emphasized the allocation of plug-in electric vehicle (PEV) charging infrastructure without integrating solar photovoltaic distributed generation (SPDG). This approach is insufficient for widespread PEV deployment, especially given the prevalent reliance on conventional power sources within the grid. Moreover, there is a notable gap in existing research regarding the systematic analysis of system reliability when proposing optimal locations for charging stations. Our model addresses these gaps by integrating renewable energy sources with the deployment of PEVs, providing a holistic approach that optimizes both systems simultaneously. To do this, this study is conducted in two distinct stages. Firstly, it focuses on the optimal placement of PEV charging stations (PEVCSs) in conjunction with SPDG units. By utilizing RESs, the study aims to mitigate the environmental effects associated with charging stations. This approach not only supports sustainability goals but also reduces the dependence on fossil fuels and minimizes greenhouse gas emissions. Secondly, the research examines the impact of combined PEV charging stations and distributed generation (DG) units on the reliability of the distribution network (DN). This comprehensive assessment ensures that the deployment of PEVCSs is optimized to maximize renewable energy integration while maintaining the reliability of the overall system. The study evaluates various scenarios to determine the best strategies for integrating these technologies, considering factors such as load demand, energy supply variability, and network stability. By addressing both the environmental impact and system reliability, this study provides a more holistic approach to deploying PEV charging infrastructure. It bridges the gap in the existing literature by offering a model that supports the sustainable growth of electric vehicle usage and ensures the stability and reliability of the power distribution network. This dual focus on optimal placement and reliability assessment makes the study a significant contribution to the field of renewable energy integration and electric vehicle infrastructure development.

Existing studies often exhibit a limited focus on integrated approaches and fail to adequately consider the variability of RESs. They also tend to lack adaptability to different geographic and climatic conditions and insufficiently utilize real-time data for optimization. Additionally, while some research considers the impact of integrating PEVs and RESs with the grid, this aspect is not comprehensively addressed in many existing studies. In contrast, our work provides a comprehensive and integrated model that overcomes these limitations. Our approach involves advanced optimization techniques that take into account the variability of RESs, making the system adaptable to different geographic and climatic conditions. Furthermore, we incorporate real-time data and smart grid technologies, enabling dynamic optimization and more efficient energy management. Moreover, our study extends to scrutinizing the impact of integrating PEVs and RESs on system reliability. We examine critical reliability indicators, including the System Average Interruption Frequency Index (SAIFI), System Average Interruption Duration Index (SAIDI), Customer Average Interruption Duration Index (CAIDI), Expected Energy Not Supplied (EENS), and Average Energy Not Supplied (AENS). By evaluating these indicators, we ensure that our integrated model not only enhances renewable energy utilization but also maintains and potentially improves the overall reliability of the power DN. This holistic approach provides a robust framework for optimizing the deployment of PEV charging infrastructure while supporting the broader goals of sustainability and reliability in the power grid. Our work represents a significant advancement over existing studies by addressing the key limitations and offering a more adaptable, data-driven, and reliable solution for integrating renewable energy with electric vehicle charging infrastructure.

1.1 Motivations and Key Contributions

The increasing penetration of PEVs presents both opportunities and challenges for modern distribution networks (DNs). As global efforts to reduce carbon emissions intensify, the transportation sector's shift towards electrification is crucial. PEVs are central to this transition, offering substantial environmental benefits by reducing reliance on fossil fuels. However, the integration of PEVs into DNs introduces complexities that must be addressed to ensure reliable and efficient power delivery. One of the primary challenges is the significant impact of uncoordinated PEV charging on DN stability and performance. Unmanaged charging can lead to substantial increases in peak demand, exacerbating power losses, and voltage deviations, and potentially causing thermal overloads in network components. These issues underscore the necessity for optimized deployment strategies for PEVCSs to mitigate adverse effects on the grid.

The motivation for this study is driven by the need to develop a robust framework for the strategic placement of PEVCSs, considering the integration of RESs such as solar-powered distributed generation (SPDG) units. The incorporation of SPDG units addresses the heightened energy demand from PEVs, contributing to the sustainability and reliability of DNs. By leveraging renewable energy, this approach not only enhances the environmental benefits of PEVs but also reduces the dependency on traditional power generation sources. Furthermore, the study aims to introduce novel methodologies for evaluating and ranking potential locations for PEVCSs using two-loss sensitivity factors (LSFs). These factors provide a systematic means of identifying critical load buses, facilitating more effective

decision-making in the placement of PEVCSs. The motivation extends to assessing the impact of combined PEVCS and SPDG deployment on the overall reliability and stability of the DN, ensuring that the system can accommodate the evolving demands of electric vehicle infrastructure. In addition to these technical aspects, the research is motivated by the broader goal of supporting policymakers and industry stakeholders in the large-scale deployment of PEV infrastructure. By providing detailed insights and practical solutions, the study aims to contribute to the development of sustainable urban mobility systems and the advancement of smart grid technologies.

The key contributions of this research work are delineated as follows:

- This research introduces a groundbreaking approach that addresses several critical issues simultaneously by leveraging AHA for the optimal allocation of PEVCSs and SPDG units. The integration of RESs with PEV infrastructure not only mitigates environmental impacts but also enhances the sustainability and efficiency of the energy distribution network. The novel utilization of AHA in this context demonstrates its versatility and potential to solve complex, multidimensional optimization problems.
- The artificial hummingbird algorithm is applied to optimize the deployment of PEV fast charging stations within a DN incorporating solar photovoltaic-based distributed generation units. This approach mimics the behavior of hummingbirds to efficiently navigate and find optimal solutions for placing PEV charging stations in proximity to renewable energy generation sites. By leveraging this algorithm, the study aims to enhance the sustainability and efficiency of PEV integration into the electrical grid, promoting renewable energy utilization and reducing carbon emissions effectively
- The study presents a robust model for determining the optimal locations of fast-charging stations, encompassing three key objectives. Beyond merely optimizing the location, the model meticulously considers the operational parameters of the distribution network (DN). It achieves this by implementing penalties for exceeding predefined safe operational limits, ensuring the model is attentive to potential system safety impacts.
- In this research, a notable contribution lies in the introduction of two-loss sensitivity factors (LSFs). These factors are specifically developed to assess and rank load buses based on their criticality within a power distribution network. By leveraging these LSFs, researchers can effectively prioritize load buses that are most suitable for the installation of PEV charging stations. This prioritization is crucial as it optimizes the selection process by narrowing down the search space for optimal placement locations. Consequently, the application of these LSFs enhances the efficiency and effectiveness of the optimization process, ensuring a more targeted approach towards deploying PEV charging infrastructure.
- This research focuses on quantifying the impact of integrating PEVs into the DN on system reliability. It involves a detailed analysis to measure how the presence of PEVs affects reliability metrics within the DN. By systematically quantifying these changes, the study aims to offer valuable insights into how PEVs influence the stability and efficiency of the power distribution network, providing critical information for future planning and optimization strategies in the energy sector.
- Incorporating real-time data and smart grid technologies, our model allows for dynamic optimization, enhancing energy distribution efficiency and system responsiveness.

The progression of this research is meticulously planned across several sections to achieve the outlined objectives. Section 2 will delve into the modeling of PEV load and solar photovoltaic-based distributed generation, providing a foundational understanding of their interaction. A detailed explanation of the voltage profile, VSI, and reliability indices is mentioned in Section 3. Following this, Section 4 will present a comprehensive mathematical formulation of the problem, including objective functions, and constraints, thereby establishing the technical framework of the study. Section 5 is dedicated to introducing and elaborating on the proposed optimization methodology, a cornerstone of this research. The pivotal findings and their implications will be thoroughly discussed in Section 6, which is central to articulating the research outcomes. Finally, Section 7 will offer a summative overview, encapsulating the key conclusions and contributions of the research and setting a stage for future study endeavors in this domain.

2. Methodology

To assess the optimal location of charging stations within the DN, it is crucial to evaluate the system's operational efficacy, particularly under the increased load conditions resulting from the growing number of PEVs. This assessment involves examining various critical operational characteristics, including the additional power loss incurred by the PEV load, the bus voltage profile, the VSI, the average VDI (AVDI), and the overall power losses. A key factor in this analysis is the peak PEV load at any given time, which is directly influenced by the charging rate. Table 2 provides

a detailed breakdown of the charging rates for PEVs. Additionally, this section outlines the methodology used to calculate the aforementioned distribution network parameters. This methodology includes a clear and concise explanation of the analytical approach adopted, which is essential for determining the network's capacity to handle the increased demand and for identifying the most efficient locations for PEV charging stations. By incorporating these elements, the study aims to ensure that the DN can support the additional load from PEVs while maintaining optimal operational performance.

Table 2. Various levels of charging PEVs

Charging levels	Rating
AC level-I	120V, 1.4 kW, 12 A or 120V, 1.9 kW, 16 A
AC level-II	240 V,18.2 kW, 80 A
AC level-III	480 V, 20 kW
DC fast charging	1000 V, 500 A, 50 - 350 kW

2.1 Modeling of PEV Load Demand

For an accurate quantification of power loss within the DN, it is essential to conduct a load flow analysis. This analysis evaluates the augmented burden imposed by PEVs on charging stations. In this study, the PEV load is calculated using a probabilistic PEV load modeling approach as outlined in [65], with a particular focus on DC fast charging for PEVs. An in-depth assessment strategy for EV load, as illustrated in Fig. 1, is employed. This strategy involves the incorporation of various factors, such as the probability fleet of daily travel distances [66], the likelihood of driving at specific time intervals [67], and the classification of different PEV types. To model these factors effectively, the daily driven mileage probability curve, which may follow an exponential distribution, is represented in Fig. 2. This distribution is formulated mathematically in (1). Additionally, Eqn. (2) is used to calculate the driven mileage weighted probability for each histogram interval. Here, DM_{avg} represents the average driven miles for the interval between two consecutive points, N and $N+1$. This modeling approach enables a detailed and realistic representation of PEV load demand, crucial for the accurate evaluation of system performance under varying PEV charging scenarios.

$$P(x) = 0.0296\exp(-0.0296x) \tag{1}$$

$$Prob(DM_{avg}) = \int_{N}^{N+1} P(x)dx \tag{2}$$

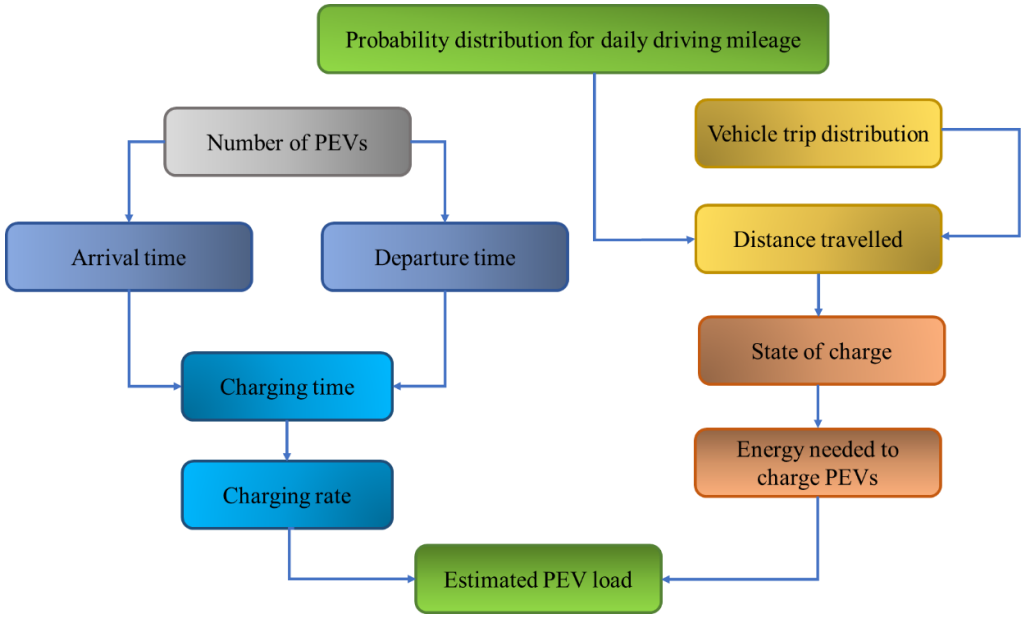

Fig. 1. Strategy for estimating the PEV load

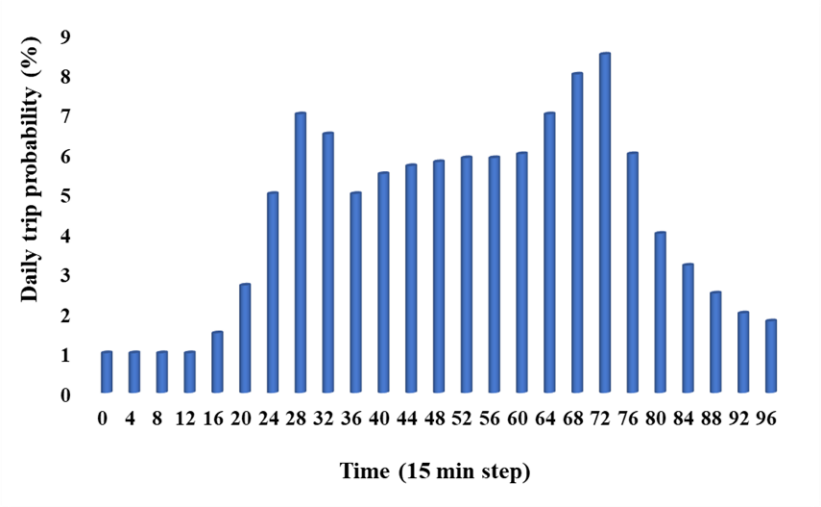

Fig. 2. Daily driven mileage probability

Furthermore, the modeling process must account for each time instant's driving probability ρ_{ti} associated with the all-electric range of the vehicle. This probability ρ_{ti} also indicates the times when the PEV is likely to return to the charging facility. To estimate the expected mileage of the EV at each time instant, the daily average driven mileage DM_{avg} is multiplied by the likelihood of driving at any given time instant ti, as articulated in (3). Subsequently, Equation (4) is employed to calculate the State of Charge (SOC) of a PEV's battery. The driver must initiate a charging session as soon as the EV battery's SOC reaches its minimum threshold SOC_{min}. The charging should continue until the battery achieves its maximum targeted SOC SOC_{max}. Additionally, considering the EV's arrival time t_A and departure time t_D at the charging station, the total duration of charging can be determined as $t_D - t_A$. This comprehensive modeling approach incorporates critical factors such as driving probability, mileage, and SOC dynamics, providing a nuanced understanding of PEV charging behavior and its implications for the distribution network.

$$DM_{avg}^{PEV}(t) = DM_{avg} \times \rho_{ti} \tag{3}$$

$$SOC(t) = SOC(t-1) - \left(\frac{\int_{t-1}^{t} DM_{avg}^{PEV}(h)dh}{AER_{PEV}}\right) \tag{4}$$

Consequently, the power provided by the charging station to the PEV at any given time t can be mathematically represented by Eqn. (5), where PEV_{CR} denotes the charging rate, and Δt symbolizes the time duration. This equation effectively captures the instantaneous power delivery dynamics during the charging process. Building upon this, Eqn. (6) is formulated to calculate the expected PEV charging requirement over the charging interval. This calculation incorporates the daily mileage probability DM_{avg}, providing a more comprehensive view of the charging demand. Moreover, to account for the collective demand of all PEVs, the total anticipated PEV demand is expressed in Eqn. (7). In this eqn., P_{dem}^{PEV} represents the cumulative PEV demand at any time t, and N_{PEV} signifies the total number of EVs that are simultaneously charging. This approach allows for a detailed assessment of the overall PEV charging load on the system, considering both individual vehicle requirements and the collective demand posed by multiple vehicles. By integrating these calculations, the study offers a holistic understanding of PEV charging patterns and their cumulative impact on the power grid.

$$P_{avg}^{PEV}(t) = PEV_{CR} \times \Delta t \tag{5}$$

$$\langle P_{avg}^{PEV}(t) \rangle = P_{avg}^{PEV}(t) \times \rho\left(DM_{avg}^{PEV}\right) \tag{6}$$

$$P_{dem}^{PEV} = \sum_{n=1}^{N_{PEV}} P_{dem}^{PEV}(n) \tag{7}$$

2.2 Modeling of Solar PV Distributed Generation

To accurately model solar photovoltaic power generation, the primary unknown variables, such as irradiance and solar cell temperature, need to be considered. Mathematical modeling is essential to estimate the PV output power at a given time using Eqn. (8) [57].

$$P_{Solar\ PV}(t) = SI(t) \times P_{Solar\ PV} \tag{8}$$

where, $P_{Solar\ PV}(t)$ represents the power output of solar PV at t^{th} hour, $SI(t)$ represents the values of solar irradiance (SI) at each time instant shown in Fig. 3. and $P_{Solar\ PV}$ is the endpoint power output of solar PV which can be computed using Eqn. (9).

$$P_{Solar\ PV} = N_{Solar\ PV} \times FF \times V_{SI} \times I_{SI} \tag{9}$$

where, $N_{Solar\ PV}$ denotes the number of solar panels used, and FF is abbreviated for the fill factor which can mathematically given in Eqn. (10).

$$FF = \frac{V_{max} \times I_{max}}{V_{OC} \times I_{SC}} \tag{10}$$

where, maximum voltage and current are represented by V_{max} and I_{max}, respectively. V_{OC} and I_{SC} stands for the open circuit voltage and short circuit current of the Solar PV panel, respectively.

Moreover, voltage at specific solar irradiance can be computed using Eqn. (11).

$$V_{SI} = V_{OC} - V_{TC} \times T_{cell} \tag{11}$$

where, V_{TC} is the temperature coefficient of voltage and T_{cell} denotes the temperature of the solar cell in degree celsius. The current produced at specific solar irradiance can be computed using Eqn. (12).

$$I_{SI} = SI_{avg} \times \left(I_{SC} + I_{TC} \times (T_{cell} - 25)\right) \tag{12}$$

where, SI_{avg} represents the mean value of solar irradiance and I_{TC} is the temperature coefficient of current.

The temperature of the solar cell can be calculated using Eqn. (13).

$$T_{cell} = T_{ambient} + \left(SI_{avg} \times \frac{T_{nominal} - 20}{0.8}\right) \tag{13}$$

where, $T_{ambient}$ denotes the ambient temperature, and $T_{nominal}$ denotes the nominal temperature.

Additionally, the modeling of solar irradiance merits special attention. A beta distribution is suggested in [68]. This distribution yields a probability density function specifically for solar irradiance, encapsulated in Eqn. (14). The adoption of the beta distribution in modeling irradiance provides a nuanced and probabilistic approach, allowing for a more accurate and representative understanding of solar energy availability and its impact on PV generation.

$$f(SI) = \begin{cases} \frac{\Gamma(\alpha_{SI} + \beta_{SI})}{\Gamma(\alpha_{SI})\Gamma(\beta_{SI})} \times SI^{(\alpha_{SI}-1)} \times (1 - SI)^{(\beta_{SI}-1)}, & if\ 0 \le SI \le 1;\ \alpha_{SI} \ge 0;\ \beta_{SI} \ge 0 \\ 0, & otherwise \end{cases} \tag{14}$$

where, α_{SI} and β_{SI} represent the shape parameters of the beta function, and their expressions can be found in Eqn. (15) and Eqn. (16), respectively.

$$\mu_{SI} = \frac{\alpha_{SI}}{\alpha_{SI} + \beta_{SI}} \tag{15}$$

$$\sigma_{SI} = \sqrt{\frac{\mu_{SI}(1 + \mu_{SI})}{\alpha_{SI} + \mu_{SI}}} \tag{16}$$

Where, μ_{SI} and σ_{SI} represent the mean and standard deviation (SD) of SI.

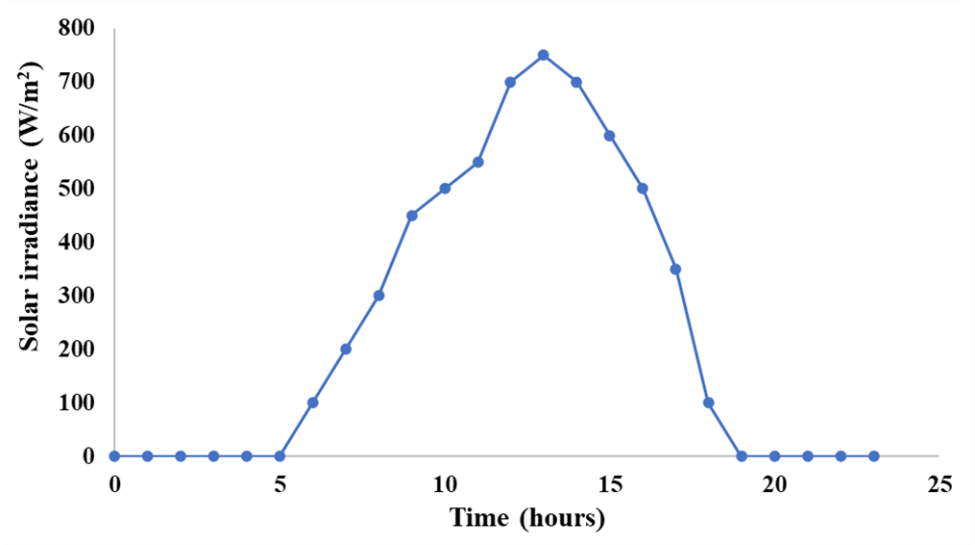

Fig.3. Daily solar irradiance profile

2.3 Loss Sensitivity Factor

In this study, two innovative Loss Sensitivity Factors (LSFs) are proposed aimed at assessing the criticality of load buses within the distribution network. These factors are crucial for identifying optimal locations for PEV charging stations. By quantifying the severity of load buses, our approach aims to refine and narrow down the search space, thereby optimizing the selection process for PEV charging station placement. This targeted approach enhances the efficiency of the optimization process, ensuring that PEV infrastructure is strategically located to minimize network stress and maximize operational effectiveness. Integrating these novel LSFs enables a more nuanced evaluation that considers both existing network conditions and future load impacts from PEVs, supporting sustainable and reliable power distribution.

The first LSF, denoted as LSF_1, is derived by calculating the first derivative of power loss $P_{l,k}$ with respect to the voltage at a particular bus V_q. This derivative is ascertained based on constants $P_{eff/q}$, $Q_{eff/q}$, and R_k. The resulting expression for LSF_1 can be articulated as follows:

$$LSF_1 = \frac{\partial P_{l,k}}{\partial V_q} = -2 \times R_k \times \left(\frac{P_{eff/q}^2 + Q_{eff/q}^2}{V_q^3}\right) \tag{17}$$

where, V_q represents the voltage of the bus q, and $P_{l,k}$ and $Q_{l,k}$ are the active and reactive power loss of the k^{th} line which can be mathematically written in (18) and (19), respectively.

$$P_{l,k} = I_k^2 \times R_k = \left(\frac{P_{eff/q}^2 + Q_{eff/q}^2}{|V_q|^2}\right) \times R_k \tag{18}$$

$$Q_{l,k} = I_k^2 \times X_k = \left(\frac{P_{eff/q}^2 + Q_{eff/q}^2}{|V_q|^2}\right) \times X_k \tag{19}$$

where, $P_{eff/q}$ and $Q_{eff/q}$ represent the total effective active and reactive power loads, respectively, which are present beyond node q. R_k and X_k represent the resistance and reactance of the k^{th} line.

The values of LSF_1 indicate the extremes of the performance index, with buses having the most negative LSF_1 values identified as prime candidates for PEV charging installation, prioritizing them at the top of the LSF_1 list. Conversely, buses with less negative LSF_1 values are ranked lower, signifying their lower sensitivity or suitability for PEV charging installation compared to higher-ranked buses. This prioritization strategy ensures that PEV charging stations are strategically placed on buses where their installation would have the greatest impact on network performance and efficiency.

The second LSF (LSF_2) is computed by taking the first derivative of $P_{l,k}$ with respect to $Q_{eff/q}$, as indicated in (20).

$$LSF_2 = \frac{\partial P_{l,k}}{\partial Q_{eff/q}} = \frac{2 \times R_k \times Q_{eff/q}}{V_q^2} \quad (20)$$

To ensure an informed and balanced approach in selecting optimal locations and sizes for PEV charging installations, candidate buses are chosen based on sensitivity indices, specifically emphasizing buses with the highest positive values of LSF_2. These buses are prioritized at the top of the LSF_2 ranking due to their heightened sensitivity to the impacts of PEV charging installations on network performance. Conversely, buses with lower positive values of LSF_2 are positioned lower in the ranking, indicating their reduced sensitivity to these installations. To maintain fairness and inclusivity in the selection process, candidate buses are selected from both LSF_1 and LSF_2 lists. This approach ensures consideration for various network configurations, including buses with fixed and switched capacitors. The selection starts from the top of these lists and encompasses approximately 50% to 55% of the total number of buses within the system as potential candidates for PEV charging installation.

The chosen candidate buses, identified through a comprehensive analysis of LSF_1 and LSF_2, are then integrated into the optimization algorithm as control variables using Eqn. (21). This integration facilitates a systematic consideration of these buses in the optimization process, ensuring that the placement of PEV charging stations optimally balances network performance, reliability, and operational efficiency. By leveraging sensitivity indices and systematic integration into the optimization framework, this approach aims to enhance the overall effectiveness and sustainability of PEV infrastructure deployment in electrical distribution systems.

$$C = \{x: x \in (X \cup Y)\} \quad (21)$$

In this context, C represents a set of control variables, while X and Y denote the sets of candidate buses determined by LSF_1 and LSF_2, correspondingly.

3. Explanation of Voltage Profile, VSI, and Reliability Indicators

This section provides a detailed mathematical modeling and explanation of the voltage profile, which illustrates the distribution of voltage levels across the network, essential for operational stability. It also covers the voltage stability index, assessing the network's capacity to maintain stable voltages under varying loads, and reliability indices such as SAIFI, SAIDI, and CAIDI, which quantify outage frequency and duration, crucial for evaluating system dependability.

3.1 Voltage Profile and VSI

In the realm of power and energy systems, the issue of voltage stability in distribution networks, especially concerning severe voltage collapse scenarios, has garnered significant attention [69]. Maintaining consistent and acceptable voltage levels at each bus node in the DN is crucial not only under normal operational conditions but also when faced with external disturbances. Voltage instability, characterized by an uncontrolled decline in bus voltages, can be triggered by various factors such as sudden load increases, faults, or multiple contingencies. To mitigate these challenges, many studies have adopted the voltage stability criterion, which ensures that bus voltages remain within predefined acceptable limits. This manuscript focuses on analyzing voltage stability by considering key variables such as the voltage profile of buses, the AVDI, the VSI, and power losses. The voltage profile of buses provides an overview of voltage levels across the network, highlighting areas that may be prone to instability. The AVDI quantifies the difference between the actual and nominal voltages, aiming to minimize this variance for a stable voltage profile. A low AVDI indicates that the system is operating close to its optimal voltage levels, reducing the risk of voltage instability. The Voltage Stability Index (VSI) is another critical measure, indicating how close the system is to a voltage collapse. By analyzing the VSI, the manuscript assesses the robustness of the network under various operating conditions and disturbances. Additionally, power losses are considered as they can impact the overall efficiency and stability of the distribution network. Minimizing power losses is essential for maintaining voltage stability and ensuring efficient energy distribution. Thus, the AVDI is defined as in (22), offering a precise metric for assessing voltage deviations and guiding efforts to maintain voltage stability. By incorporating these key variables into the analysis, the manuscript provides a comprehensive approach to understanding and enhancing voltage stability in distribution networks, addressing both theoretical and practical aspects of the issue.

$$AVDI = \frac{1}{M}\left(\sum_{i=1}^{M} \sqrt{(V_m - |V_i|)^2}\right) \quad (22)$$

where V_m is the nominal voltage and M denotes the total number of buses in DN. Moreover, this study also incorporates the VSI as defined in [53]. For a more comprehensive illustration, an example of a 2-bus system is presented in Fig. 4,

where $V_a\angle\delta_a$ and $V_b\angle\delta_b$ represent the voltages at buses a and b, respectively. This example aids in visualizing the practical application of the theoretical concepts discussed, providing a clearer understanding of the dynamics of voltage stability in distribution networks.

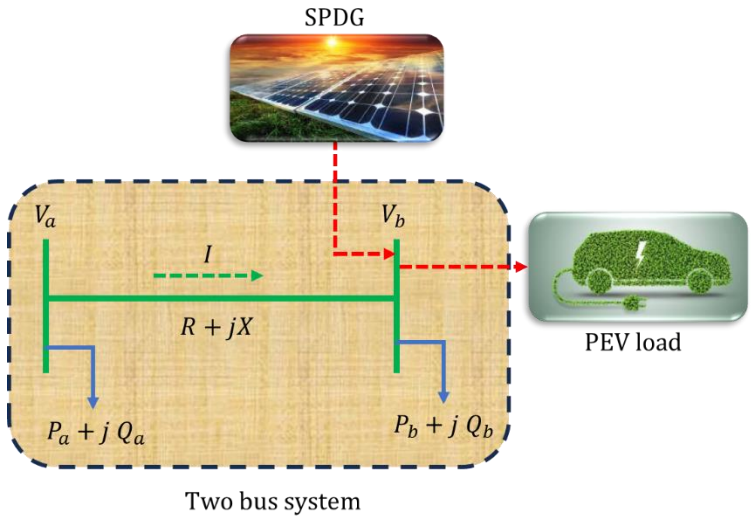

Fig. 4. Typical layout of two bus system

Eqn. (23) delineates the current flow through a branch line with resistance (R), reactance (X), and impedance (Z). The interrelation of various parameters at bus b is further elucidated in Eqn. (24). Substituting the value of current (I) into (24) and simplifying it leads to Eqn. (25), which facilitates the representation of transferable active and reactive power in Eqn. (26) and Eqn. (27), respectively. The transferable power must meet the criteria specified in Eqn. (28).
Additionally, Eqn. (28) can be reformulated into an inequality, as shown in Eqn. (29), which is referred to as the VSI. The Voltage Stability Index (VSI) demonstrates an inverse relationship with active power. This means that as active power increases, the VSI decreases. This relationship indicates that the system becomes less stable as more active power is drawn or supplied. However, this inverse relationship has a critical limit. If the active power exceeds a specific threshold, the VSI may drop to a dangerously low level. Once this threshold is surpassed, the system's stability is compromised, which can lead to a collapse. This collapse could manifest as voltage instability, resulting in voltage sags, power outages, or even a complete failure of the electrical grid. To ensure the system operates safely and efficiently, it is crucial to monitor the active power and maintain it within safe limits. Exceeding these limits can have severe consequences, highlighting the importance of maintaining a balance between power demand and supply to avoid potential system failures.

$$I = \frac{V_a - V_b}{R + jX} \tag{23}$$

$$P_b - jQ_b = V_b^* \times I \tag{24}$$

$$V_b^4 + 2V_b^2(P_bR + Q_bX) - V_a^2V_b^2 + (P_b^2 + Q_b^2)|Z|^2 = 0 \tag{25}$$

$$P_b = \frac{-cos\theta_z V_b^2 \pm \sqrt{cos\theta_z V_b^4 - V_b^4 - |Z|^2 Q_b^2 - 2V_b^2 Q_b X + V_a^2 V_b^2}}{|Z|} \tag{26}$$

$$Q_b = \frac{-sin\theta_z V_b^2 \pm \sqrt{sin\theta_z V_b^4 - V_b^4 - |Z|^2 P_b^2 - 2V_b^2 P_b R + V_a^2 V_b^2}}{|Z|} \tag{27}$$

$$\begin{pmatrix} cos\theta_z V_b^4 - V_b^4 - |Z|^2 Q_b^2 - 2V_b^2 Q_b X + V_a^2 V_b^2 \geq 0 \\ sin\theta_z V_b^4 - V_b^4 - |Z|^2 P_b^2 - 2V_b^2 P_b R + V_a^2 V_b^2 \geq 0 \end{pmatrix} \tag{28}$$

$$2V_a^2V_b^2 - 2V_b^2(P_bR + Q_bX) - (P_b^2 + Q_b^2)|Z|^2 \geq 0 \tag{29}$$

3.2 Reliability Indicators (RI)

The growing demand for fast-charging PEVs has introduced significant challenges to distribution networks. These networks are tasked with managing the increased and often unpredictable load demands resulting from unplanned charging activities. This surge in load demand can strain the system, leading to adverse effects on its reliability. When the load demand increases rapidly due to PEV charging, the DN may struggle to maintain stability and performance. This can result in compromised reliability measures, which are critical for ensuring consistent and dependable power delivery to consumers. As a result, there is often an increase in system outages and interruptions, leading to consumer dissatisfaction. To evaluate and quantify the reliability of a DN, Reliability Indices (RIs) are used. These indices can be classified into two main categories: customer-oriented RIs (CORIs) and energy-oriented RIs (EORIs). The former includes SAIFI, SAIDI, and CAIDI, whereas the latter comprises EENS and AENS. The data required for the reliability evaluation of the proposed DN has been derived from preceding studies [70]. These studies provide valuable insights and historical data that are essential for accurately assessing the reliability of the system under the new challenges posed by the increasing demand for fast-charging PEVs.

RIs play a crucial role in evaluating the performance and dependability of distribution networks. These indices are significantly influenced by key statistical variables, particularly the failure rate and the duration of outages. The failure rate refers to the frequency at which faults or failures occur within the network, while the duration of outages indicates the amount of time the system is non-operational during each failure event. Therefore, these variables must be adjusted to accommodate the additional PEV load and SPV-based distributed generation impacts. The failure rate and the duration of interruptions specific to a bus in the network can be quantified using Eqn. (30) and (31).

$$\delta_{PEV} = (P_{base} + \Delta P_{PEV}) \frac{\delta_{base}}{P_{base}} \tag{30}$$

$$T_{PEV} = (P_{base} + \Delta P_{PEV}) \frac{T_{base}}{P_{base}} \tag{31}$$

The base values of active power demand, failure rate, and outage duration for the DN are represented by P_{base}, δ_{base}, and T_{base}, respectively. ΔP_{PEV} symbolizes the integrated active power load introduced by electric vehicles within the distribution system.

The CORIs encompass SAIFI, SAIDI, and CAIDI, while EORIs include EENS and AENS. SAIFI is determined by the number of disruptions experienced by consumers within a specific time frame. SAIFI deteriorates as the system experiences an increase in disruptions and the number of customers, which can be expressed as shown in (32).

$$SAIFI = \frac{\sum(\delta_{PEV} \times C_i)}{\sum(C_i)} \tag{32}$$

The variable C_i denotes the number of customers connected to the *i*-th bus, factoring in the addition of PEVCSs and SPV-based distributed generations. SAIDI, alternatively, is calculated by considering the total duration of interruptions experienced by each customer over a specific period, taking into account the effect of EV charging loads. This index offers insights into the network's performance relative to the length of service interruptions, as expressed in (33).

$$SAIDI = \frac{\sum(T_{PEV} \times C_i)}{\sum(C_i)} \tag{33}$$

CAIDI is calculated by assessing the average failure rate, the additional time required for this rate to escalate due to the increased load from electric vehicles, and the total number of customers affected. It signifies the average duration a customer is expected to wait for service restoration post an interruption, as depicted in (34).

$$CAIDI = \frac{\sum(T_{PEV} \times C_i)}{\sum(\delta_{PEV} \times C_i)} \tag{34}$$

Equation (35) defines the EENS within the network. It is calculated as in (35), providing a measure of the energy shortfall.

$$EENS = \sum(P_{PEV} \times T_i) \tag{35}$$

The term PEV refers to the DN's load after the integration of EVs. In contrast, AENS is an index that reflects the requested load at a specific bus, offering a perspective on the quantum of energy that remains unsupplied within a certain timeframe due to escalating charging demands. The formulation for AENS is presented in (36).

$$AENS = \frac{\sum(P_{PEV} \times T_i)}{\sum(C_i)} \tag{36}$$

4. Problem Formulation

Determining the optimal placement of charging stations within DNs involves a comprehensive approach that takes into account several critical objective functions. Key objectives include minimizing power loss across the network, which ensures efficient energy distribution and reduces operational costs. Additionally, assessing voltage sensitivity is crucial to maintaining voltage stability and ensuring reliable power supply to all users. Operational conditions, including fluctuating demand patterns and the integration of RESs, also play a significant role in shaping the optimal placement strategy. Balancing these multiple objectives and constraints ensures a robust and efficient deployment of charging stations, enhancing the overall performance and reliability of the distribution network.

4.1 Objective Functions

A pivotal objective of this research is to minimize the additional power loss that arises from integrating new charging stations into the DN. Power loss minimization is crucial as it fine-tunes the placement of these stations to ensure they have the least disruptive impact on the network's overall efficiency. Concurrently, the system's voltage sensitivity plays a critical role in identifying optimal locations for charging stations, as it significantly influences the reliability and stability of the system. The primary aim of this research is to improve the voltage profile and stability of the DN while concurrently minimizing power loss. Achieving this requires a comprehensive load flow analysis. This analysis should consider two scenarios: a base case representing the network without any PEV load and another case that includes the total PEV load incorporated into the network. Comparing these two scenarios helps to understand the impact of PEV integration on the DN. An objective function that effectively captures these critical aspects—minimizing power loss, minimizing voltage deviation, and enhancing voltage stability—is formulated and presented in Eqn. (37). This objective function is central to the study, enabling a balanced approach that not only optimizes the distribution network's performance but also enhances its capacity to accommodate the evolving demands of PEV integration. This process must also adhere to various constraints and conditions such as physical limitations of the infrastructure, budgetary restrictions, and regulatory requirements. By addressing these multiple objectives and constraints, the research aims to ensure that the deployment of charging stations is both efficient and sustainable, enhancing the overall reliability and performance of the distribution network.

$$Objfcn = min\left(\alpha_1 f_{p,loss} + \alpha_2 f_{AVDI} + \alpha_3 f_{VSI}\right) \tag{37}$$

$$f_{p,loss} = \frac{P_{loss}^{PEV,SPV}}{P_{loss}^{base}} \tag{38}$$

$$P_{loss}^{base} = \sum_{j=1}^{k} G_{ij}\left[V_i^2 + V_j^2 - 2V_i V_j cos\left(\theta_i - \theta_j\right)\right] \tag{39}$$

$$f_{AVDI} = \frac{AVDI_j^{PEV,SPV}}{AVDI_j^{base}} \tag{40}$$

$$AVDI_j^{base} = \frac{1}{M}\left(\sum_{i=1}^{M} \sqrt{(V_m - |V_i|)^2}\right) \tag{41}$$

$$f_{VSI} = 1 - \frac{\sum_{j=2}^{N} VSI_j^{PEV,SPV}}{\sum_{j=2}^{N} VSI_j^{base}} \tag{42}$$

$$VSI_j^{base} = \left[|V_i|^4 - 4\left(X_{ij}P_i - R_{ij}Q_i\right)^2 - 4\left(R_{ij}P_i + X_{ij}Q_i\right)|V_i|^2\right] \tag{43}$$

Eqn. (37) precisely defines the objective function for the proposed methodology, emphasizing a dual-focus approach. The first component of this function is dedicated to computing the total system power loss. This calculation is crucial because the integration and optimal placement of PEVCSs significantly affect the DN's current and voltage profiles. By accurately modeling these factors, Eqn. (37) helps identify the optimal locations for PEVCSs, aiming to minimize total system power loss while maintaining robust network performance. This bifurcated focus ensures that the proposed methodology not only addresses the immediate impact of PEV integration but also contributes to the long-term sustainability and efficiency of the distribution network.

The second part of the objective function addresses the voltage profile and voltage stability issues, which are especially pertinent to the integration of PEVs through charging stations at different nodes along the distribution lines. The AVDI (f_{AVDI}) in relation to the system's nominal voltage (V_m), offers a quantifiable assessment of the impact of charging station allocation on the voltage profile. This is mathematically formulated in Eqn. (40). Additionally, the VSI is a critical parameter for ensuring reliable and secure operations within the DN. The VSI is calculated based on several factors,

including voltage, active and reactive power flow, and the resistance and reactance between the sending and receiving ends of the system, as delineated in Eqn. (43). In the formulation of Eqn. (37), each objective component is accorded equal importance. This is achieved by setting the weighting coefficients (α_i) for each component such that their cumulative value equals 1, i.e., $\sum_{i=1}^{3} \alpha_i = 1$. Consequently, $\alpha_1 = \alpha_2 = \alpha_3 = 1/3$. The computing process of the VSI is illustrated in the flowchart presented in Fig. 5.

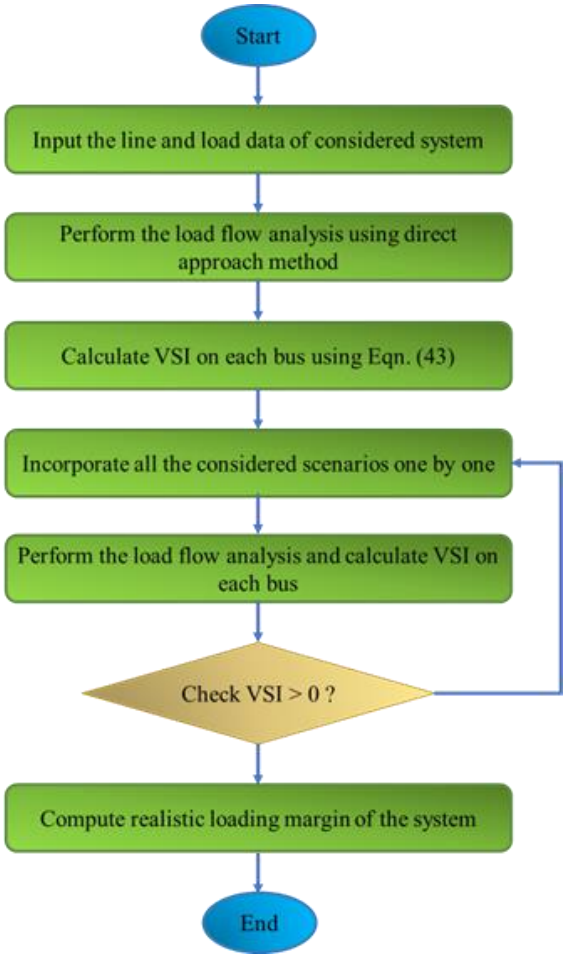

Fig. 5. Computation of voltage profile and VSI

4.2 Constraints

The objective function, as delineated in Eqns. (37-43), is subject to adherence to a set of critical system constraints to ensure operational integrity and safety. One such constraint pertains to the permissible voltage limits at each node in the DN. Specifically, the voltage at node i (V_i) during operation must be maintained within a specified range, bounded by the maximum (V_{max}^i) and minimum (V_{min}^i) voltage limits, as formulated in Eqn. (44). Maintaining voltage within these limits is crucial to avoid under-voltage and over-voltage conditions, which can cause equipment malfunction or damage. Another significant constraint arises from the increased PEV load through the charging stations, which consequently impacts the thermal limit of line conductors. To mitigate the risk of thermal overload, it is imperative that the optimizer complies with Eqn. (45). This equation ensures that the power flow (P_j) through any line section j does not exceed the maximum permissible power limit P_j^{max}, which is determined based on the sustainable thermal limit of the conductors. This constraint is crucial for preventing potential thermal damage to the network infrastructure and maintaining the overall safety and efficiency of the power DN. Compliance with this constraint prevents thermal overload, thereby protecting the network infrastructure from damage and ensuring long-term reliability.

$$V_{min}^i \leq V_i \leq V_{max}^i \tag{44}$$

$$P_j \leq P_j^{max} \tag{45}$$

$$P_{gi} = P_{di} + V_i \sum_j V_j Y_{ij} cos\left(\delta_i - \delta_j - \theta_{ij}\right) \tag{46}$$

$$Q_{gi} = Q_{di} + V_i \sum_j V_j Y_{ij} sin\left(\delta_i - \delta_j - \theta_{ij}\right) \tag{47}$$

$$\sum(\eta_{CR}^{PEV} PEV_{CR} \Delta t) + SOC_{initial} \geq SOC_{max}^{PEV} \tag{48}$$

$$|V_i|^4 - 4\left(X_{ij}P_i - R_{ij}Q_i\right)^2 - 4\left(R_{ij}P_i + X_{ij}Q_i\right)|V_i|^2 \geq 0 \tag{49}$$

The power flow within the distribution network is regulated by constraints detailed in Eqn. (46) and Eqn. (47). These equations encompass active and reactive power generation P_{gi}, Q_{gi}, and demand P_{di}, and Q_{di} for each *i*-th bus, respectively. Additionally, $V_i \angle \delta_i$ and $V_j \angle \delta_j$ signify the voltages at respective buses, while $Y_{ij} \angle \theta_{ij}$ represents the admittance of the (*i*,*j*)-th term in the bus admittance matrix. Furthermore, Eqn. (48) ensures that each PEV is fully charged upon returning from the charging station, considering charging efficiency (η_{CR}^{PEV}) of 96%. PEV_{CR} represents the charging rate, which depends on the charging level, Δt is the charging duration, and $SOC_{initial}$ and SOC_{max}^{PEV} denotes the initial and maximum possible SOC of the PEV battery, respectively. For enhanced reliability, stability, and operational security of the distribution network, it is essential that the f_{VSI} at the bus where the PEV charging station is located is greater than zero. This ensures that the voltage at this critical node remains stable despite the additional load from charging activities. The minimum VSI value among all buses is used to represent the system's overall VSI. A positive system VSI indicates that all buses in the network are stable, preventing voltage collapse and ensuring the network can reliably handle the increased demand. Maintaining a positive VSI across the network is crucial for preventing operational disruptions and ensuring continuous, secure power distribution. Hence, it adheres to the constraint stated in Eqn. (49).

The PEV battery, a critical element of the system, must operate within specific technical constraints, including the minimum and maximum SOC levels as specified by the manufacturers. Eqn. (50) calculates the SOC of the PEV battery at a particular time t, considering the charging or discharging over a period Δt. Eqn. (51) establishes the permissible SOC limits, ensuring adherence to these manufacturer specifications. Furthermore, Eqns. (52) and (53) define the energy constraints for the battery's charging and discharging within the given time interval Δt. These constraints are essential for maintaining the battery's health, optimizing its performance, and preventing degradation. Adhering to these constraints ensures the battery operates efficiently and sustainably, thereby enhancing the overall reliability and effectiveness of the PEV charging infrastructure. This careful management of the SOC and energy flow contributes significantly to the system's robustness and longevity.

$$SOC_{PEV}^{t} = SOC_{PEV}^{t-1} + \frac{PEV_{CR} \times \Delta t \times \eta_{CR}^{PEV} - PEV_{DCR} \times \Delta t / \eta_{DCR}^{PEV}}{B_{CR}^{PEV}} \tag{50}$$

$$SOC_{min}^{PEV} \leq SOC_{PEV}^{t} \leq SOC_{max}^{PEV} \tag{51}$$

$$0 \leq PEV_{DCR} \times \Delta t \leq B_{CR}^{PEV} \times \left(SOC_{PEV}^{t+1} - SOC_{PEV}^{min}\right) \tag{52}$$

$$0 \leq PEV_{CR} \times \Delta t \leq B_{CR}^{PEV} \times \left(SOC_{PEV}^{t+1} - SOC_{PEV}^{min}\right) \tag{53}$$

5. Optimization Algorithm

The quest for optimal placement of charging stations along distribution lines has seen an array of computational techniques being employed by researchers. These techniques range from classical optimization algorithms to evolutionary algorithms, PSO, sequential quadratic programming, ant colony optimization, GAs, flower pollination, and cuckoo search algorithms. Addressing the limitations and gaps identified in existing literature, this manuscript presents a comparative analysis of PEV charging station and SPV-based distributed generation placement techniques, with a specific focus on ensuring voltage stability. For this purpose, the study examines the efficacy of three distinct algorithms: the AHA, the BESA, and the Salp Swarm Algorithm (SSA).

5.1 Artificial Hummingbird Algorithm (AHA)

Launched towards the end of 2021, the AHA is a cutting-edge bio-inspired optimization tool that finds applications across various engineering fields. It draws inspiration from the ingenious activities of hummingbirds [71] and mirrors other optimization strategies by establishing distinct exploration and exploitation stages. It integrates three key elements, food sources (FSs), hummingbirds, and a visit table, to facilitate the solution of diverse optimization problems. Hummingbirds are renowned for their ability to assess fundamental aspects of FSs, such as nectar quality,

production rate, and the recency of their last visit to a particular flower. They possess a remarkable memory for tracking the location and replenishment rate of food sources and are capable of sharing this information with other hummingbirds in their vicinity. The algorithm's visit table records the frequency of visits to each food source and is updated after every iteration cycle. The AHA employs three distinct foraging styles: directed, territorial, and migrant foragings. These styles influence the algorithm's development, guiding the search process through different approaches. The mathematical models for these three foraging strategies are presented below, outlining the unique mechanisms each style brings to the optimization process. This innovative approach enables the AHA to effectively navigate the solution space, optimizing the placement of PEVCSs and SPV-based DG in a manner that enhances voltage stability and overall system efficiency.

5.1.1 Initialization

A group of *n* hummingbirds is arbitrarily assigned to *n* FSs as indicated.

$$x_i = lb + r \times (ub - lb) \quad i = 1,2,3 \ldots\ldots n \tag{54}$$

lb and ub represent the lower and upper limit, x_i is the position of i^{th} food source, r is a random variable whose values lie in the range of 0 and 1.

The visit tables for the FSs can be initialized in the following manner:

$$vt_{i,j} = \begin{cases} 0 & if\ i\ is\ not\ equal\ to\ j \\ null & if\ i = j \end{cases} \quad i = 1,2,3 \ldots\ldots n \quad j = 1,2,3 \ldots\ldots n \tag{55}$$

5.1.2 Guided foraging (GF)

Every hummingbird visits the nectar spot with the greatest nectar. Hummingbirds travel in three directions: axially, diagonally, and omnidirectionally. The axial flight can be defined in the following manner:

$$D_i = \begin{cases} 1 & if\ i\ equal\ to\ randi([1,d]) \\ 0 & else \end{cases} \quad i = 1,2,3 \ldots\ldots d \tag{56}$$

The diagonal flight can be defined as:

$$D_i = \begin{cases} 1 & if\ i\ equal\ to\ y(j), j\ belongs\ to\ [1,k], y = randperm(k), k \in [2, \lceil r_1 * (d-2) \rceil + 1] \\ 0 & else \end{cases} \quad i = 1,2,3 \ldots\ldots d \tag{57}$$

The omnidirectional flight can be mathematically illustrated as:

$$D_i = 1 \quad i = 1,2,3 \ldots\ldots d \tag{58}$$

where $randperm(k)$ constructs a number permutation from 1 to k and $randi([1,d])$ produces an arbitrary number between 1 and d and r_1 is an arbitrary number in the range of (0, 1]. The mathematical equations for demonstrating focused foraging behavior with a suitable FS can be written as follows:

$$v_i(t+1) = x_{i,int}(t) + b * D * \left(x_i(t) - x_{i,int}(t)\right) \tag{59}$$

$$b = N(0,1) \tag{60}$$

where $x_{i,int}(t)$ is the location of the i^{th} hummingbird's preferred food source, and b is a factor of guiding, $N(0,1)$ is the normal distribution with SD of 1 and mean of 0, and $x_i(t)$ is the location of the i^{th} food supply at time t.

The position of i^{th}food source can be updated as follows:

$$x_i(t+1) = \begin{cases} x_i(t) & f(x_i(t)) \le f\left(v_i(t+1)\right) \\ v_i(t+1) & f(x_i(t)) > f\left(v_i(t+1)\right) \end{cases} \tag{61}$$

If the nectar-refilling rate of the candidate FS (CFS) is greater than that of the present FS, the hummingbird quits the current FS and sucks at the CFS defined by (61).

5.1.3 Territorial foraging (TF)

A hummingbird can swiftly shift to a nearby spot in search of a potentially superior food source compared to its current one. The subsequent mathematical equations delineate the local foraging approach of hummingbirds and the adequacy of a food supply in their territorial foraging strategy:

$$v_i(t+1) = x_i(t) + g * D * x_i(t) \tag{62}$$

$$g = N(0,1) \tag{63}$$

The variable g represents a territorial factor characterized by a normal distribution with a mean of 0 and a SD of 1, denoted as $N(0,1)$.

5.1.4 Migration foraging (MF)

The transition of a hummingbird from the nectar source with the lowest refilling rate to a randomly generated new source can be described in the following manner:

$$x_{worst} = lb + r \times (ub - lb) \tag{64}$$

x_{worst} denotes the food with the least nectar replenishment rate.

A hummingbird engaged in both directed foraging and TF would systematically visit each FS, treating it as the target source based on the visit table during each iteration, provided there are no replacements for all FSs. Assuming a 50% success rate in choosing between directed and TF, and a 50% success rate in visiting every other source during directed foraging, a migratory foraging approach becomes necessary to break stagnation and expand the search area. Consequently, the proposed population size specification for the migration coefficient is as follows:

$$M = 2n \tag{65}$$

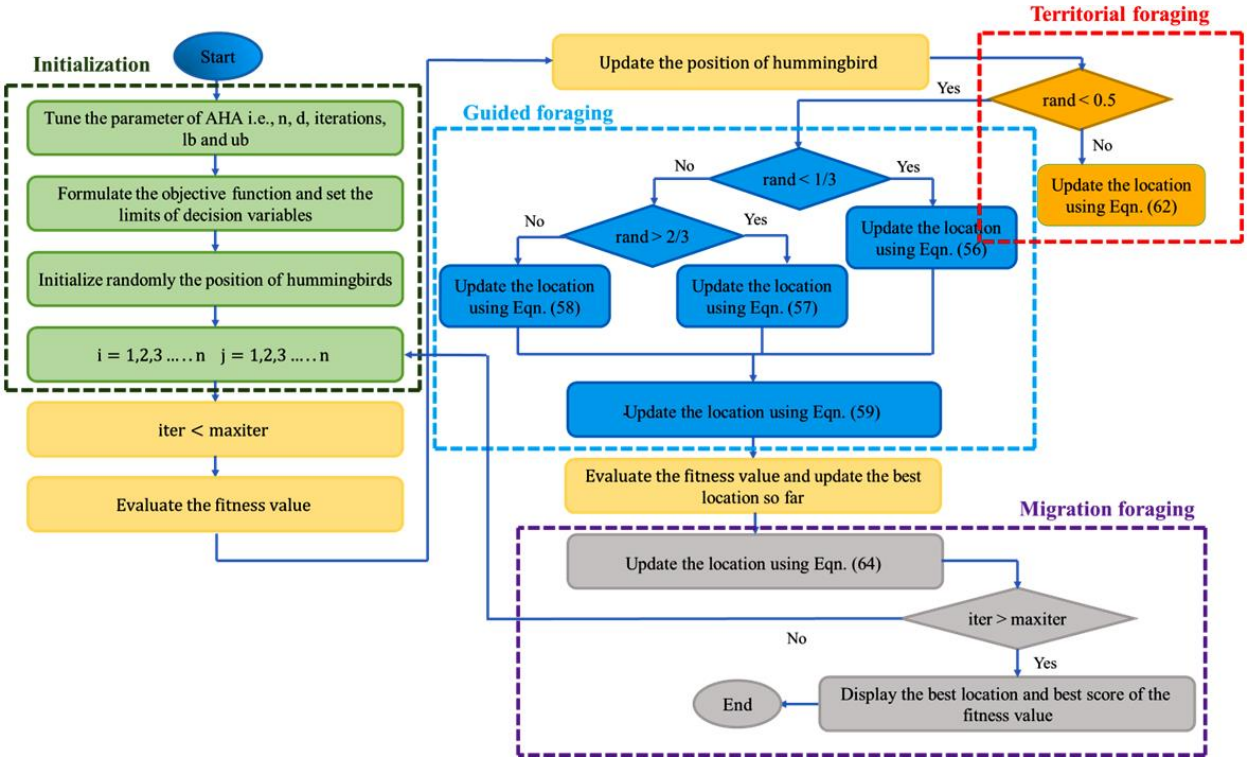

Fig 6. Flow chart of Artificial Hummingbird Algorithm for the optimization problem

5.2 Bald Eagle Search Algorithm (BESA)

The BESA impacted the hunting behavior of bald eagles (BEs) [72]. As part of the hunt tactics, space selection, scouring, and swooping in on the quarry are all employed.

Space Selection: The bald creates the amount of space arbitrarily using the previously sought information using (66).

$$Q_{n,j} = Q_b + \alpha \times r\left(Q_{mean} - Q_j\right) \tag{66}$$

As in the earlier BESA, an updated parameter, α, is used to resolve location shifts and can be conveyed using (67) is similar to a predetermined weight.

$$\alpha = \frac{\left(1.5\times(max_{iter}-t+1)\right)}{max_{iter}} \tag{67}$$

This suggested parameter influences the exact position of BEs and enhances the exploration and exploitation features of BESA. r is an integer whose value lies between 0 and 1, Q_b indicates the best search, Q_n denotes the new search, and Q_{mean} indicates that the eagles have retained all the information from the previous search.

Scouring stage: To expedite their hunt for prey in the designated area, bald eagles move in a circular path using (69). The position of the bald eagle is adjusted at every moment using Eqn. (70) – Eqn. (72).

$$Q_{j,n} = Q_j + n(j) \times \left(Q_j - Q_{j+1}\right)Q_b + m(j) \times \left(Q_j - Q_{mean}\right) \tag{68}$$

$$m(j) = \frac{mr(j)}{max|mr|} \quad n(j) = \frac{nr(j)}{max|nr|} \tag{69}$$

$$mr(j) = r(j) \times sin\left(\delta(j)\right),\ nr(j) = r(j) \times cos\left(\delta(j)\right) \tag{70}$$

$$\delta(j) = \alpha \times \pi \times rand \tag{71}$$

$$r(j) = \delta(j) \times R \times rand \tag{72}$$

where α lies between 5 and 10, R varies within the range of 0.5 and 2.

Swooping-stage: In this stage, the eagles begin to swoop towards their quarry from an optimal search posture using (73)-(76).

$$Q_{j,n} = rand \times Q_b + m_1(j) \times \left(Q_j - C_1 \times Q_{mean}\right) + n_1(j) \times \left(Q_j - C_1 \times Q_b\right) \tag{73}$$

$$m_1(j) = \frac{mr(j)}{max|mr|} \quad n_1(j) = \frac{nr(j)}{max|nr|} \tag{74}$$

$$mr(j) = r(j) \times sinh\left(\delta(j)\right),\ nr(j) = r(j) \times cosh\left(\delta(j)\right) \tag{75}$$

$$\delta(j) = \alpha \times \pi \times rand\ ,\ \ r(j) = \delta(j) \tag{76}$$

The values of C_1 and C_2 lie between 1 and 2. The steps involved in the implementation of BESA are displayed below (Fig. 7).

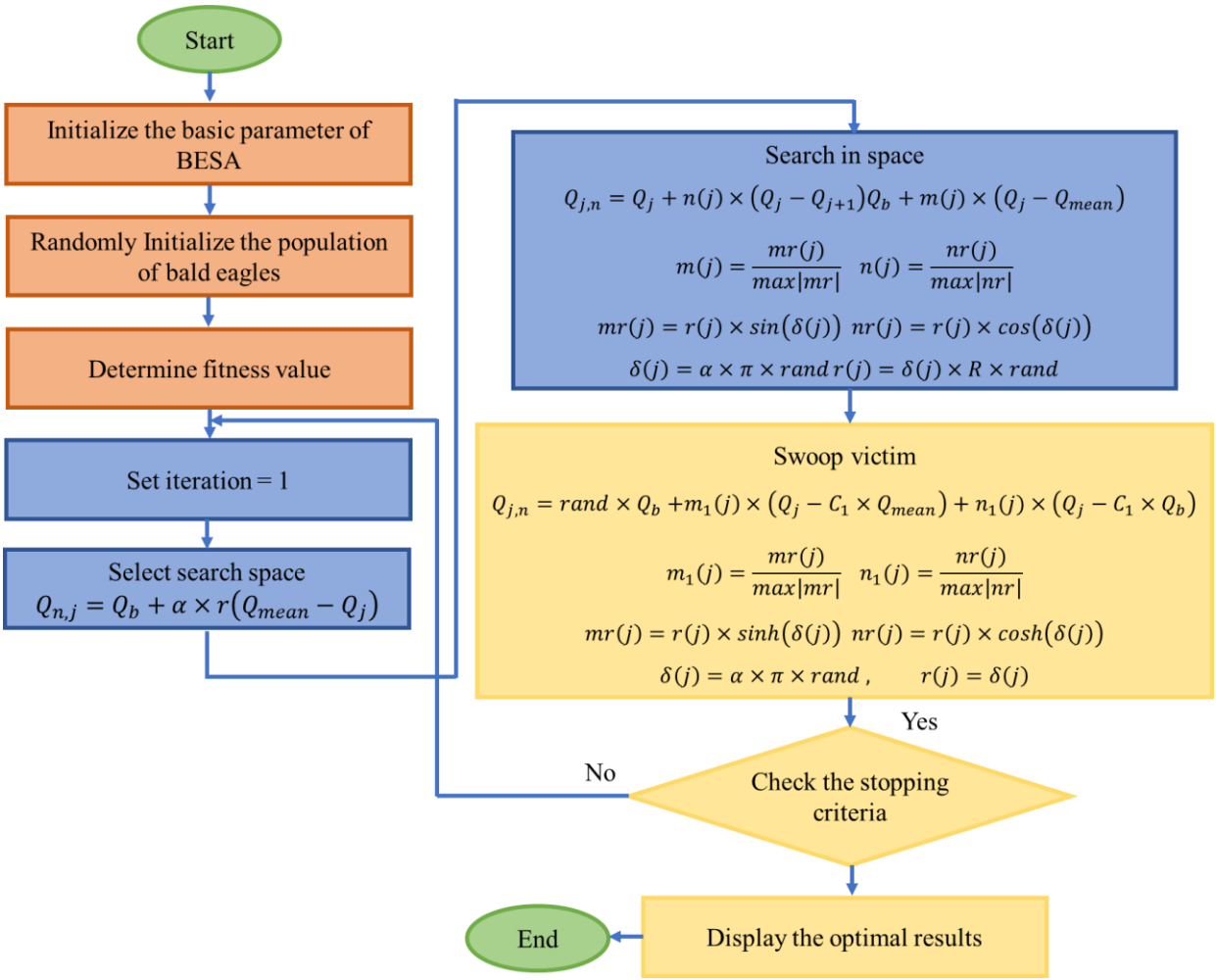

Fig 7. Flow chart of BESA for the proposed problem

5.3 Salp Swarm Algorithm (SSA)

Mirjalili et al. devised a population-oriented method known as the SSA in 2017. This algorithm models the hunting behavior of salps in seawater [73]. The salp at the top of the sequence will clear the way for further salps that come afterwards

In *m*-dimensional space, salp's location is represented, with *n* representing the variables in a specific scenario. Consequently, a matrix with two dimensions, referred to as z, stores the precise positions of all salps. The equation governing SSA can be written in the following manner:

$$z_n^1 = \begin{cases} R_n + r_1[(ub_n - lb_n)r_2 + lb_n], & r_3 \geq 0 \\ R_n - r_1[(ub_n - lb_n)r_2 + lb_n], & r_3 < 0 \end{cases} \tag{77}$$

where, z_n^1 signifies the location of the leader salp, whereas the position of target food can be symbolized as R_n. ub_n and lb_n represents the variable upper and lower limits.

In the context of SSA, the coefficient r_1 serves a crucial function by ensuring a balanced equilibrium between exploration and exploitation capabilities. It is illustrated as:

$$r_1 = 2 * \exp\left(-\left(\frac{4b}{B}\right)^2\right) \tag{78}$$

Here, b represents the current iteration, whereas B signifies the total iteration.

The parameters r_2 and r_3 are uniformly generated with values ranging from 0 to 1. These parameters determine both the step size and the direction (positive or negative infinity) of the subsequent point in the *n*-th dimension.

The positions of the follower salps undergo adjustments based on Newton's Second Law of Motion, a process that can be mathematically described by (79).

$$z_n^i = \frac{1}{2}at^2 + v_o t \tag{79}$$

where, $i \geq 2$, v_o represents the initial velocity, and $a = \frac{v_{final}}{v}$, where $v = \frac{x - x_o}{t}$

The computation time is influenced by the number of iterations, and when the conflict between iterations is equal to one and $v_o = 0$, the equation will manifest in the following manner:

$$z_n^i = \frac{1}{2}(z_n^i + z_n^{i-1}) \tag{80}$$

The mathematical representation of salp chains can be achieved through (77-80).

The use of Eqn. (81) enables the balancing of exploration and exploitation methods.

$$A(t) = A_{min} + \left(\frac{A_{max} - A_{min}}{B_{max}}\right) \times b \tag{81}$$

A_{max} and A_{min} are the upper and lower values of the operator A, respectively. The flow chart of SSA is represented in Fig. 8.

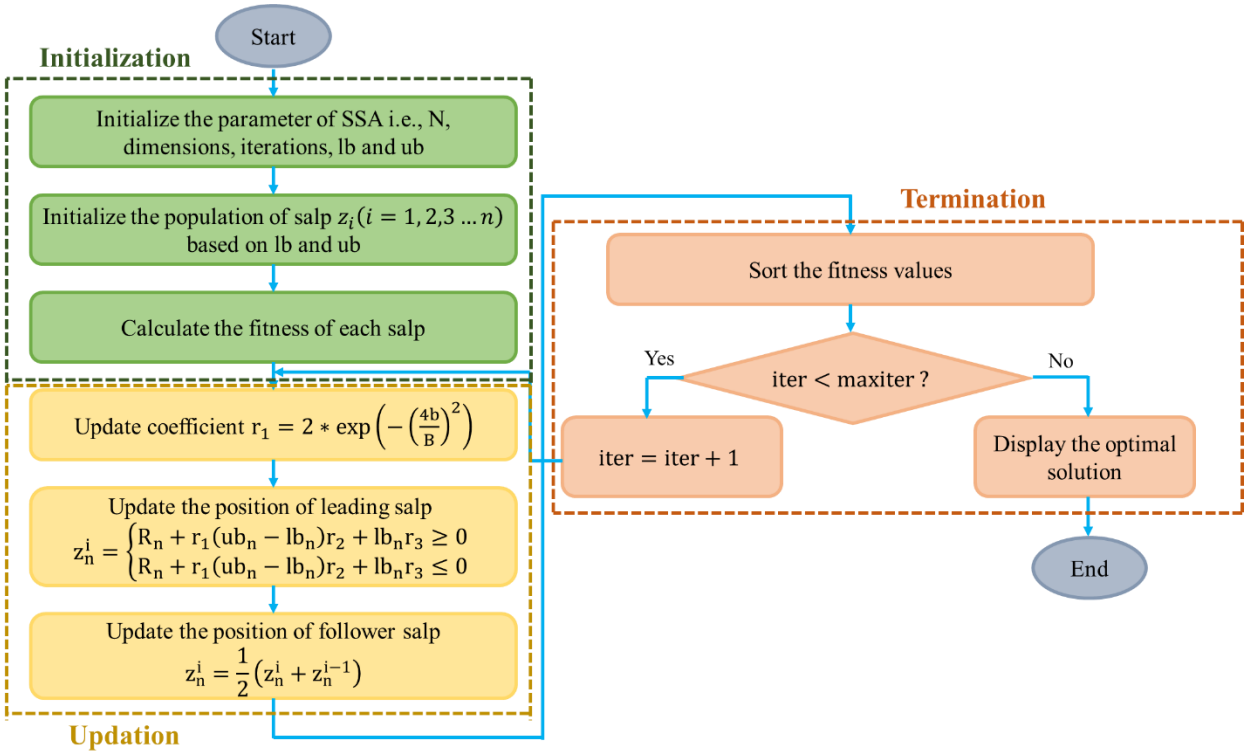

Fig. 8. Proposed salp swarm algorithm flow chart

6. Simulation Results

This section presents a comprehensive investigation of the simulation results of the study. Initially, we delve into the ranking of buses in the DN based on loss sensitivity factors, followed by implementation of the proposed AHA on benchmark functions. The AHA is then applied to the IEEE 33-bus system to assess its effectiveness. Additionally,

this section provides an in-depth evaluation of the impacts resulting from the integration of PEVCSs and SPDG units on the reliability indices of the standard system, which includes SAIFI, SAIDI, and CAIDI, among others.

6.1 Results of Loss Sensitivity Factors

Table 3 outlines the results of the LSFs for the IEEE 33-bus radial distribution systems. These indices are pivotal in assessing the implications of PEV integration on the distribution network. Buses ranked higher in the LSF list are deemed more favorable for the installation of PEV charging stations due to their higher tolerance to additional load. In contrast, buses with lower sensitivity to PEV integration are positioned lower in the ranking. Table 3 specifically illustrates the arrangement of load buses in relation to LSF1 and LSF2, with a focus on an IEEE 33-bus DN. Notably, the first 17 rows of load buses, as indicated by both LSF1 and LSF2, are identified as prime candidates for the establishment of PEV charging stations. This strategic selection of load buses is instrumental in pinpointing the most beneficial locations for PEV charging infrastructure, thereby optimizing the distribution system's capacity to support the burgeoning demand for EV charging facilities.

Table 3. Various levels of charging PEVs

LSF1				LSF2			
Order (bus number)	Value	Order (bus number)	Value	Order (bus number)	Value	Order (bus number)	Value
19	-2.78	20	-0.01	29	0.942	33	0.0012
29	-0.99	22	-0.01	30	0.277	20	0.0011
30	-0.31	21	-0.01	18	0.133	21	0.0011
25	-0.16	5	-0.02	6	0.065	22	0.0011
24	-0.15	13	-0.03	24	0.029	13	0.0010
18	-0.14	33	-0.04	25	0.029	5	0.0009
6	-0.07	12	-0.03	7	0.008	12	0.0009
32	-0.04	28	-0.03	32	0.007	11	0.0006
8	-0.03	9	-0.03	8	0.007	27	0.0004
7	-0.03	10	-0.03	4	0.005	26	0.0004
31	-0.02	27	-0.03	14	0.004	28	0.0004
4	-0.01	17	-0.03	31	0.003	9	0.0003
14	-0.01	26	-0.03	2	0.003	17	0.0003
3	-0.02	16	-0.03	3	0.002	10	0.0003
2	-0.03	15	-0.03	23	0.001	16	0.0003
23	-0.01	11	-0.02	19	0.001	15	8.76E-05

6.2 Implementation of AHA on various unimodal and multimodal functions

The efficacy of the AHA is rigorously evaluated using a variety of benchmark functions. This exploration involves a comparative analysis of the AHA's performance against other contemporary optimization techniques, including the BESA, the SSA, and the GOA. Key performance metrics such as the best (*B*), worst (*W*), and mean (*M*) values obtained by the AHA are juxtaposed with those of the comparative algorithms. The results, including relevant algorithm parameters, are methodically documented in Table 4. This table also presents the outcomes for both unimodal (F1–F7) and multimodal (F8–F10) benchmark functions. The comparative data delineates the superior performance of the AHA technique over other meta-heuristic methods for these specific functions. The designed system is implemented on MATLAB R2018a. The Windows 10 Pro Version 21H2 (64-bit) PC with a 1.80 GHz Intel Core i7-10510U CPU and 16 GB RAM ran tests efficiently. Fig. 9 offers a detailed schematic of the IEEE 33-bus radial DN. This network comprises 33 nodes and 32 branches and operates at a capacity of 100 MVA and 12.66 kV. It supports an aggregate active power load of 3715 kW and a reactive power load of 2300 kVAR.

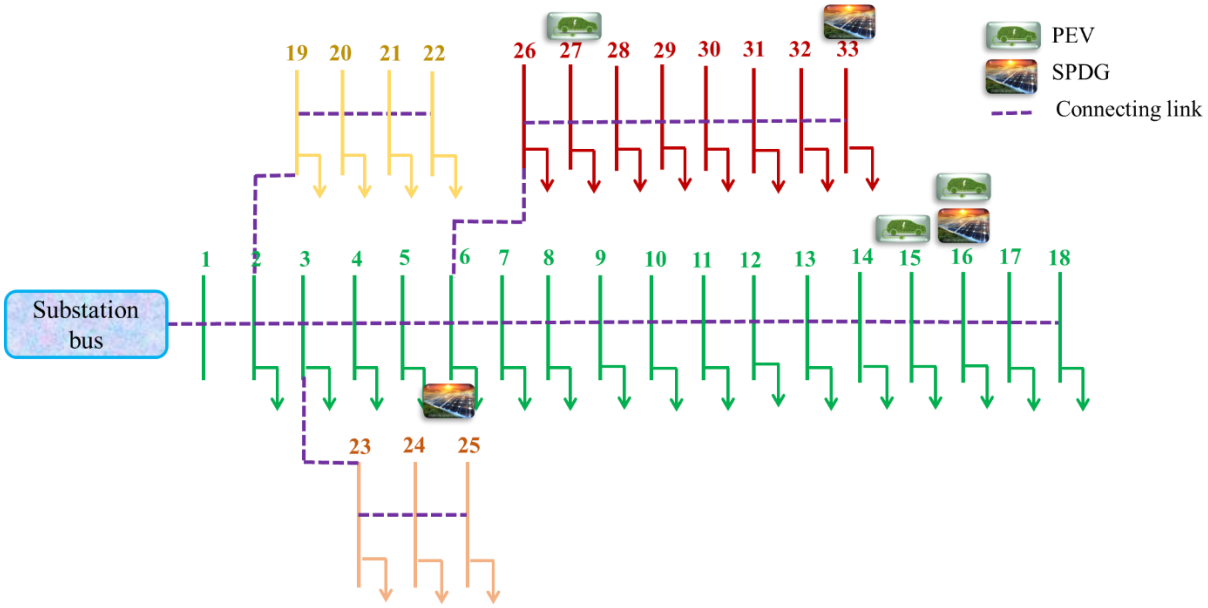

Fig. 9. Layout of IEEE 33 bus system integrated with PEVs and SPDG [74]

The PEV charging stations within this framework are designed with 30 charging points, each capable of delivering 50 kW. This configuration allows for the simultaneous charging of 30 PEVs. For optimal performance, these stations must be strategically positioned at the most suitable buses within the DN. However, the introduction of PEV charging stations incrementally increases the active power loss in the system. To effectively mitigate this issue, SPDG units are optimally placed to offset the losses incurred by the PEV charging station installations. The optimization process, aimed at minimizing power loss, is conducted using the proposed AHA method, demonstrating the algorithm's practical application in enhancing the efficiency and sustainability of the DN under the evolving demands of EV charging infrastructure.

Table 4. Implementation of the proposed approach on benchmark functions

Function		AHA	BESA	SSA	GOA
	B	0	0	1.00E−23	0.0683
F1	*W*	0	0	9.21E−21	4.4581
	M	0	0	1.92E−21	0.9876
	B	0	0	4.32E−13	0.029
F2	*W*	4.47e-303	1.37e-276	6.59E−08	79.104
	M	2.73e-304	5.83e-763	2.44E−08	10.244
	B	0	0	9.84E−18	450.35
F3	*W*	0	0	9.84E−18	4603.90
	M	0	0	6.59E−17	1789.34
	B	0	0	6.59E−17	3.0335
F4	*W*	1.60e-287	1.51e-254	1.96E−11	19.5647
	M	8.32e-287	7.54e-263	1.96E−11	9.7766
	B	23.761	23.876	25.763	25.698
F5	*W*	25.387	25.763	29.354	7522.98
	M	24.187	24.432	25.387	987.9
	B	1.43e-5	6.70e-7	0.03963	0.0203
F6	*W*	0.24934	7.86e-5	0.2283	11.0973
	M	0.03567	1.79e-5	0.10643	0.8998
	B	2.25e-6	1.54e-43	0.000837	0.0090
F7	*W*	3.10e-4	0.000456	0.009452	0.0602
	M	8.49e-5	0.000242	0.002987	0.0234
	B	-1731.28	-1777.43	-1986.38	-8903.54

F8	*W*	-1354.46	-1043.287	-1763.38	-6468.46
	M	-1543.72	-1463.298	-1876.27	-7736.46
	B	0	0	0	1.9899
F9	*W*	0	0	0	27.8687
	M	0	0	0	9.4876
	B	8.88e-16	8.88e-29	8.88e-18	1.5021
F10	*W*	20	24	32	56
	M	9	18	28	37

Prior to the deployment of PEV charging stations and SPDG units, an essential load flow study is undertaken using a direct approach to ascertain the base-case losses in the distribution network. This preliminary analysis provides a baseline for evaluating the impacts of integrating PEV charging infrastructure and SPDGs into the system. The outcomes of this initial load flow analysis reveal that the active and reactive power losses before the installation of PEV charging stations and SPDGs amount to 202.67 kW and 135.14 kVAR, respectively. These figures serve as critical benchmarks against which the effectiveness of the proposed installations can be measured. A detailed assessment of the voltage profile across the DN is also performed. The minimum voltage magnitude is observed at bus-18, registering a value of 0.9131 per unit (p.u.). This parameter is particularly important as it indicates the voltage level at the most stressed bus in the network, which can be a focal point for voltage improvement strategies.

Furthermore, the study identifies the lowest value of the VSI as 0.6953 p.u. The VSI is a key indicator of the network's ability to maintain stable voltage levels under varying load conditions. A lower VSI value can signal potential areas of vulnerability in the network's voltage stability, guiding the strategic placement of PEV charging stations and SPDGs to bolster system robustness.

6.3 Impact of PEV charging stations and SPDG units on Active and Reactive Power Loss

The integration of PEVCSs into a DN invariably leads to a rise in system power losses. This escalation is primarily attributed to the additional power consumption required for charging PEVs, which intensifies the overall demand on the network. Consequently, this heightened demand may induce a decline in the voltage profile, with increased PEV loading potentially causing voltage drops in certain segments of the network. To counteract these challenges, it is imperative to allocate PEV charging stations in an optimized and strategic manner. The objective is to mitigate the rise in power losses engendered by the charging stations, while concurrently maintaining a stable and reliable distribution system. Optimal placement of these charging stations can significantly minimize the total power losses, striking a balance between accommodating the charging needs of PEVs and preserving the network's operational integrity.

For empirical validation, the study undertakes the following case studies (CS):

- CS1: Baseline scenario before allocation of PEV charging stations and SPDG units.

- CS2: Incorporation of two PEV charging stations.

- CS3: Implementation of two SPDG units only.

- CS4: Simultaneous placement of two PEV charging stations and two SPDG units.

- CS5: Addition of three PEV charging stations.

- CS6: Integration of three SPDG units.

- CS7: Concurrent allocation of three PEV charging stations and three SPDG units.

Optimally positioned SPDGs yield several benefits for the power system. Primarily, they contribute to the reduction of power loss by generating electricity closer to load centers, thus curtailing resistive losses in distribution lines. Additionally, the strategic placement of SPDGs can enhance the voltage profile and stability within the network. By injecting power where necessary, SPDGs help maintain voltage levels within acceptable ranges and augment the VSI,

thereby reducing the risk of voltage collapse during system perturbations. The pursuit of minimizing power losses in power systems is pivotal due to its direct impact on the efficiency and cost-effectiveness of electricity distribution. By diminishing these losses, utilities can optimize resource utilization, delivering electricity more economically to end-users.

Prior to assessing the system's reliability, it is crucial to calculate key variables such as power losses, voltage levels, and the VSI. The voltage deviation index, in particular, quantifies the divergence of voltage from its nominal value, reflecting the system's ability to maintain voltage within acceptable boundaries. The reliability evaluation focuses on determining the optimum SPDG size and location, as well as gauging its influence on power loss, voltage deviation, and VSI. This comprehensive approach enables researchers to identify the most effective SPDG placements and sizes, thereby significantly enhancing the power network performance and reliability.

Table 5. Results analysis using AHA

Cases	Active power loss (kW)	Reactive power loss (kVAR)	Optimal PEV charging station				Optimal SPDG units		
			PEV location	Number of PEVs	Active power of PEVs (kW)	Reactive power of PEVs (kVAR)	Location	Size (kW)	Size (kVAR)
CS1	202.67	135.141	–	–	–	–	–	–	–
CS2	210.71	139.61	20	14	91	44.07	–	–	–
			4	19	123.5	59.81			
CS3	39.02	28.15	–	–	–	–	12	1095	530.33
							31	1173	568.11
CS4	34.99	26.72	32	13	87.83	40.9	11	833	403.44
			20	12	97.16	37.77	29	1333	645.60
			20	27	175.5	84.9			
CS5	211.76	140.91	2	31	201.5	97.59	–	–	–
			24	13	84.5	40.92			
							29	1009	488.68
CS6	24.59	17.74	–	–	–	–	24	1006	487.22
							14	670	324.49
			27	47	305.5	147.96	33	862	417.48
CS7	29.01	24.03	16	32	208	100.73	6	1225	593.29
			15	14	91	44.07	16	725	351.13

The initial active and reactive power losses, before the allocation of PEVCSs and SPDG units, were calculated to be 202.67 kW and 135.14 kVAR, respectively as indicated in Table 5. Following the allocation of two PEV charging systems in CS2, located at buses 20 and 4, there was a rise in the active and reactive power losses by 3.967% and 3.307% with respect to the base case. In this configuration, 14 PEVs were assigned to bus 20, while 19 PEVs were charged at bus 4. The active power drawn by PEVs at buses 14 and 4 was measured to be 91 kW and 123.5 kW, respectively. Additionally, the reactive power drawn by PEVs at buses 20 and 4 was estimated to be 44.07 kVAR and 59.81 kVAR, respectively. CS3 involves the placement of two SPDG units within the distribution network. Installing two type-3 SPDGs that deliver both active and reactive power into the network brings further improvements. These two SPDGs are optimally placed at bus numbers 12 and 31 in the distribution system, with their respective capacities at bus 12 being 1095 kW for active power and 530.33 kVAR for reactive power, and at bus 31 being 1173 kW for active power and 568.11 kVAR for reactive power. With this optimal configuration, the active power loss in the network is decreased to 39.02 kW, while the reactive power loss decreases to 28.15 kVAR. By introducing these SPDGs at strategic locations, the network experiences reduced power losses in terms of both active and reactive power. This outcome signifies the efficacy of the SPDGs in compensating for power demand variations and enhancing the overall efficiency and stability of the DN. Instead of individually placing PEV charging stations and SPDG units, CS4 involves the simultaneous allocation of both PEV charging stations and SPDG units. This integrated approach yields significant reductions in active and reactive power losses, which amount to 82.7% and 80.22%, respectively. In this configuration, two PEV charging stations are located at Bus 32 and Bus 20, while two SPDG units are allocated to Bus 11 and Bus 29. Bus 32 is assigned 13 PEVs, and Bus 20 is assigned 12 PEVs. The SPDG at bus 11 has an optimal capacity of 833 kW for active power and 403.4403 kVAR for reactive power, whereas the SPDG at bus 19 has a

capacity of 1333 kW for active power and 645.61 kVAR for reactive power. In CS5, the number of PEV charging stations is increased to three, located at buses 20, 2, and 24, with 27, 31, and 13 assigned PEVs, respectively. This increased quantity of PEV charging stations leads to a 4.485% increase in active power loss and a 4.27% increase in reactive power loss. Furthermore, CS6 involves the allocation of three SPDG units, which are optimally placed at buses 29, 24, and 14. The respective optimum capacities of the SPDG units at these buses are 1009 kW, 1006 kW, and 670 kW for active power, and 488.681 kVAR, 487.228 kVAR, and 324.4958 kVAR for reactive power. In CS7, three SPDG units have been installed at buses 33, 6, and 16 along with three PEV charging stations placed at buses 27, 16, and 15. The total active and reactive power losses in this scenario come out to be 29.01 kW and 24.032 kVAR which is significantly less than the base case. The varying behavior of active and reactive power loss considering different case studies is illustrated in Fig. 10.

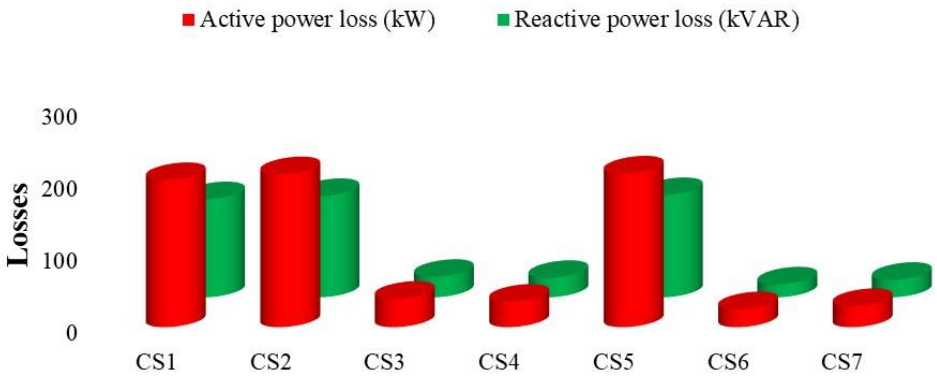

Fig. 10. Variation of active and reactive power loss in different case studies

In Fig. 11 and Fig. 12, the active and reactive power flow in all branches of the DN is shown for different case studies. With the inclusion of a PEV charging station, the active power flow increases to a higher value due to the additional load from the charging stations. However, this increased power flow is effectively managed by the optimal placement of SPDG units at specific nodes in the DN, bringing the active power flow back within allowable limits. The SPDG units act as a compensating measure, ensuring that the system remains stable and within operational constraints despite the added demand from the PEV charging station.

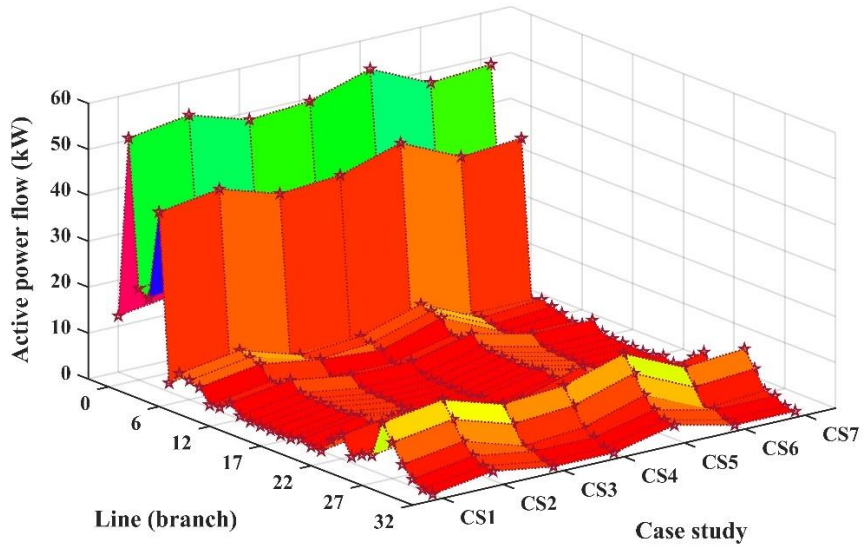

Fig. 11. Flow of active power in branches of the network

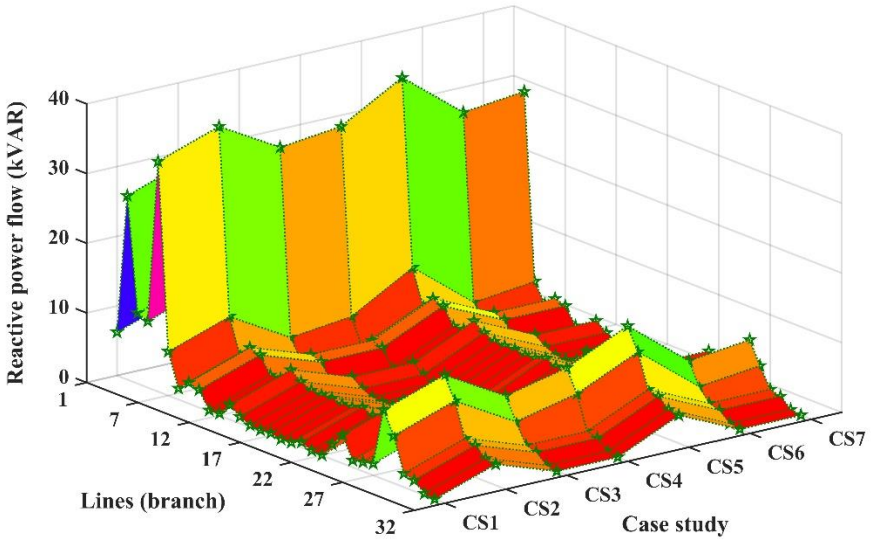

Fig. 12. Flow of reactive power in branches of the network

6.4 Impact of PEV charging stations and SPDG units on Voltage Levels and VSI

Similar to the impact on system losses, the integration of PEV charging systems has a negative impact on the voltage levels and VSI of the network. The increased load from the PEVs leads to a deterioration in the voltage profile and VSI of the distribution network. However, this negative effect is mitigated by the strategic placement of SPDG units at suitable nodes in the DN. The SPDG units compensate for the disturbances caused by the PEV charging stations, helping to maintain and improve the voltage profile and voltage stability of the network. Fig. 13 illustrates the voltage profile of the IEEE 33-bus system for considered case studies, demonstrating how the SPDG units play a crucial role in maintaining system stability and reliability in the presence of PEV charging loads. The voltage levels on all buses vary based on the DN's actual and reactive power losses. To reduce real power losses and enhance voltage levels by mitigating losses, active power support is necessary. The presence of multiple SPDGs in the system leads to an improvement in bus voltages. Moreover, it is observed that a single SPDG's size is larger than the combined size of two SPDG units. In scenario CS2, where two PEV charging units are installed at buses 20 and 4, the minimum voltage level is observed at bus 20, with a magnitude of 0.91123 p.u. This value is lower compared to the base case (CS1), indicating a decrease in voltage in comparison to the original state. The reduction in voltage is attributed to the increased power demand from PEV users, which leads to a deterioration in voltage regulation. In CS3, two SPDG units are allocated at buses 12 and 31, resulting in improved voltage levels. The minimal voltage is recorded at 0.98063 p.u., which is closer to the desired reference value. This enhancement in voltage levels is due to the contribution of SPDG units, which inject renewable energy into the system. However, the voltage levels decrease further in CS4, where two PEV charging units are optimally placed at buses 32 and 20, along with two SPDG units at buses 11 and 29. The presence of PEV loads in conjunction with SPDG units has a detrimental impact on the overall voltage profile of the DN. The combined effect of high PEV demand and SPDG injection influences the voltage regulation negatively. Despite this, the simultaneous allocation of PEV charging systems and SPDG units in the DN offers better voltage levels compared to individual placement of PEV charging units. This indicates that the benefits of SPDG units in stabilizing voltage somewhat counteract the voltage fluctuations caused by PEV charging. Furthermore, the research suggests that raising the number of SPDG units in the system enhances voltage regulation. As more SPDG units are allocated, the system experiences improved voltage levels and better voltage stability, which is beneficial for the overall health of the distribution network.

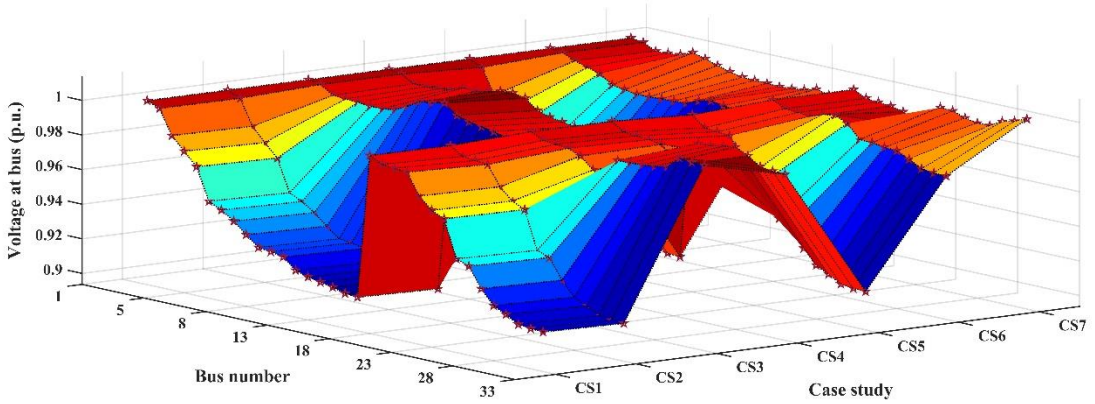

Fig. 13. Voltage levels at different buses of the system

The integration of PEVCS and DG units into the DN affects both the VSI and the voltage profile. In the base case (before the allocation of PEVs and SPDGs), the VSI value is 0.6953 p.u. With the optimal installation of two PEV charging stations in CS2 at bus 20 and 4, the VSI drops to 0.6924 p.u. On the other hand, the implementation of SPDGs in the distribution system improves the VSI. It is evident from Fig. 14 that the VSI further improves as a greater number of SPDGs are optimally placed in the DN. The variation of VSI optimized using various optimization algorithms is displayed in Fig. 15.

The placement of two SPDGs as in CS3 in the system increases the VSI to 0.8181 p.u., while the implementation of three SPDGs as in CS6 further enhances it to 0.8798 p.u. The VSI deteriorates in CS4 and CS7 in comparison to CS3 and CS6 due to the presence of PEV load, which imposes an adverse impact on the VSI. The study investigates VSI for various cases using the suggested approach and compares it with other approaches to showcase its superiority. The obtained VSI outcomes using the proposed technique and its comparison with other algorithms for the 33-bus network are given in Table 6. The VSI values indicate the voltage stability status of the system, and higher values signify better voltage stability. The analysis demonstrates that the addition of SPDGs has a positive effect on the VSI, leading to improved voltage stability in the distribution network.

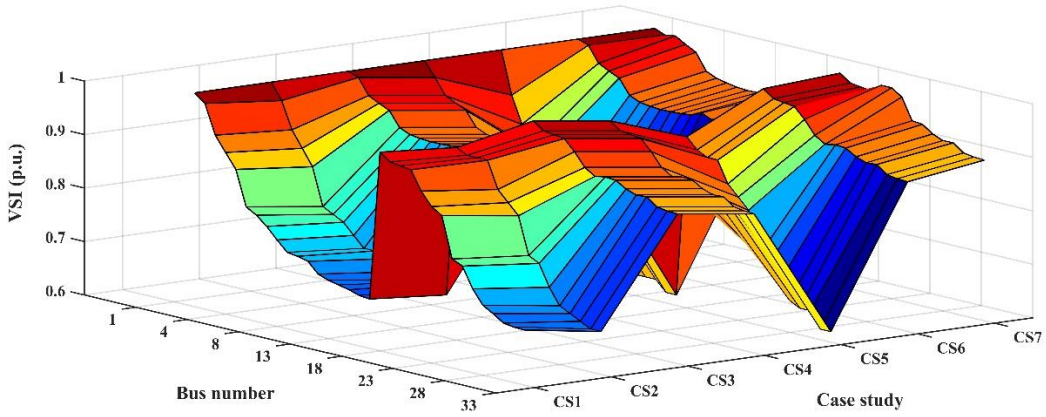

Fig. 14. Variation of VSI at different buses of the network

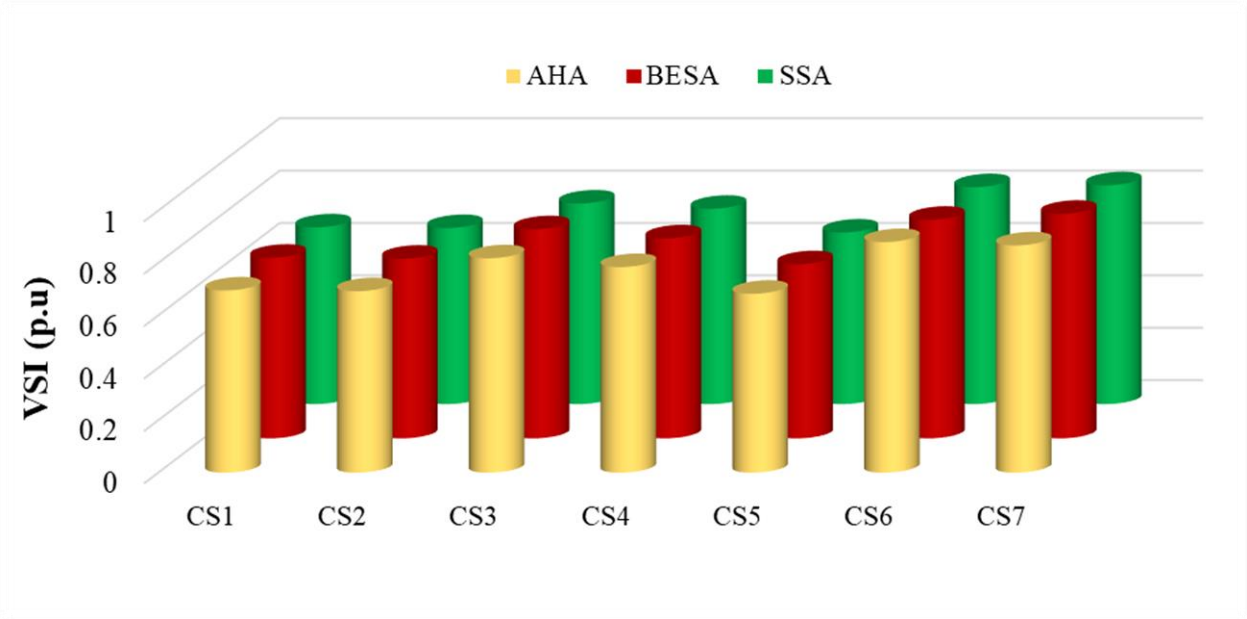

Fig. 15. Variation of voltage stability index estimated by different algorithms

Table 6. Comparison of VSI achieved using different algorithms

Scenarios	VSI (p.u)		
	AHA	BESA	SSA
CS1	0.6953	0.6893	0.6743
CS2	0.6924	0.6857	0.6717
CS3	0.8181	0.7981	0.7654
CS4	0.7845	0.7633	0.7452
CS5	0.6827	0.6645	0.6546
CS6	0.8798	0.8343	0.8278
CS7	0.8672	0.8571	0.8349

In the study, the execution times for each scenario were estimated using the proposed AHA, detailed in Fig. 16. Among all considered cases, CS1, which involves no allocation of PEV charging stations and SPDG units, has the shortest execution time, totaling 3.18 seconds. Conversely, the longest execution time is observed in CS7, taking approximately 4.59 seconds to complete the program. CS4 follows closely with an execution time of 4.43 seconds. These timings highlight the computational efficiency and variability across different scenarios evaluated in the study.

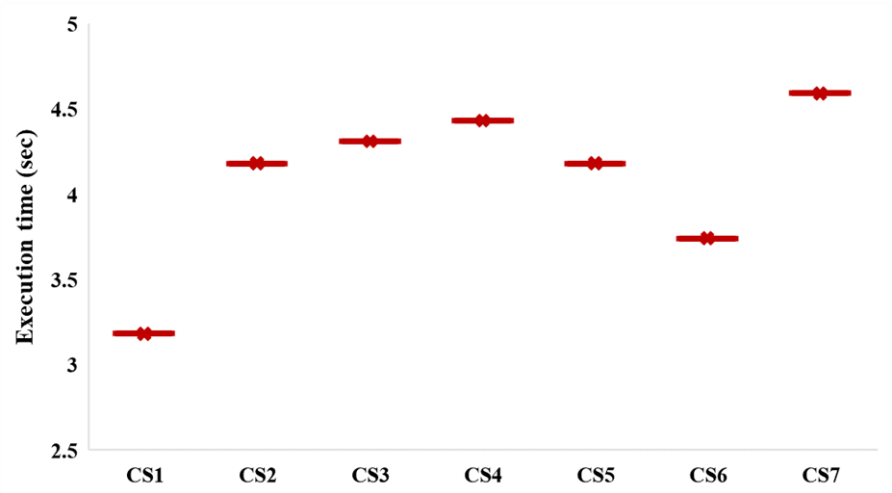

Fig. 16. Execution time taken in different case-studies

The extended execution times observed in these cases are primarily attributed to the inclusion of PEV charging stations and SPDG units, which introduce heightened computational demands and algorithmic complexities. In practical applications, execution time significantly influences the speed and efficiency of algorithm performance. This study's findings underscore that as the quantity of PEV charging systems and SPDG units rises, there is a corresponding increase in execution time. This relationship highlights the computational challenges and trade-offs involved in optimizing distribution network operations with integrated PEVs and SPDGs. Furthermore, researchers and developers should take into account these findings when integrating the proposed AHA into real-world applications. Addressing the observed execution times can lead to exploring optimization strategies aimed at enhancing operational efficiency. Additionally, Fig. 17 depicts the convergence curve of active power loss across various case studies, illustrating the gradual approach of the system toward optimal solutions through diverse optimization techniques. This visualization provides insights into the algorithm's effectiveness in minimizing active power loss and optimizing system performance under different scenarios.

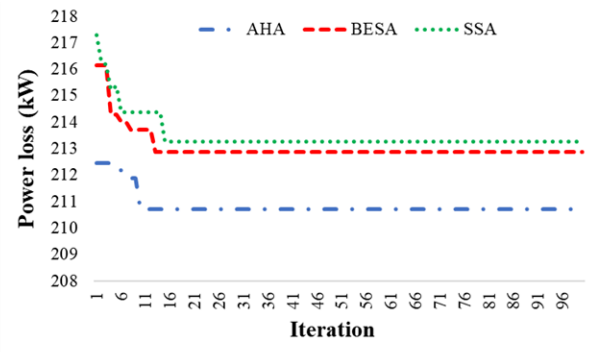

(a) 2 PEVs

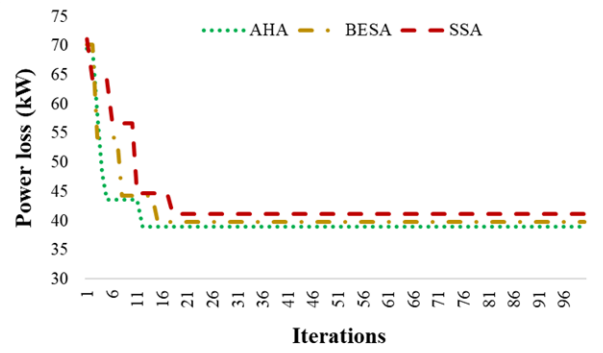

(b) 2 SPDG

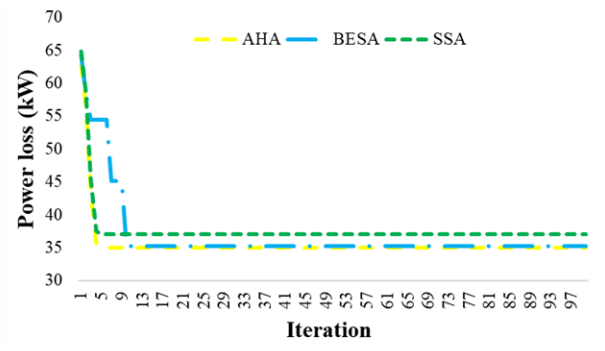

(c) 2 PEV and 2 SPDG

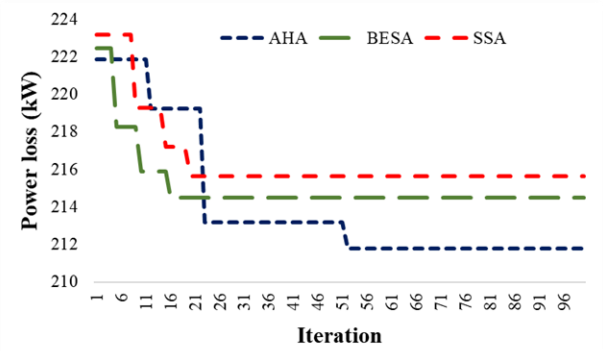

(d) 3 PEVs

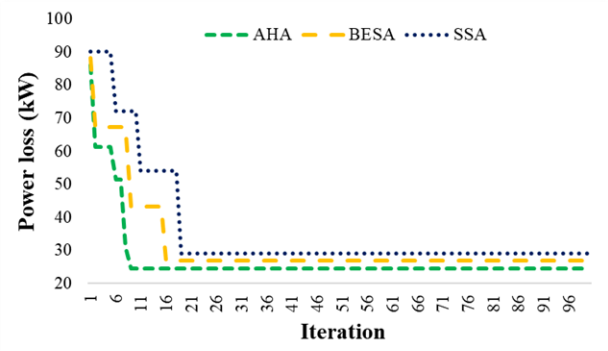

(e) 3 SPDGs

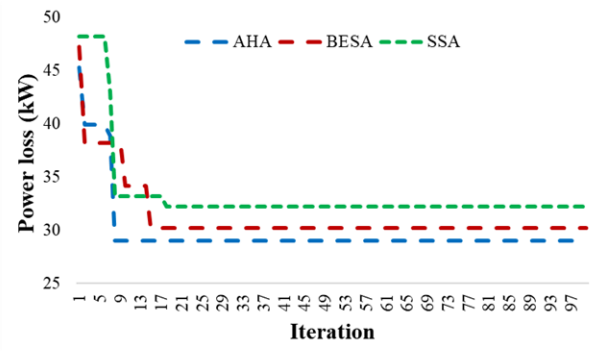

(f) 3 PEV and 3 SPDGs

Fig.17. Convergence characteristics for different case studies

6.5 Impact of PEV charging stations and SPDG units on Reliability Indicators

The aim is to showcase the impact of integrating PEVCSs and SPDG units on the system's reliability. The RIs for the electric power grid are derived from quantitative data on failure and repair rates, mean outage time, and the number of customers at various load spots. This article considers several RIs, including SAIFI, SAIDI, CAIDI, EENS, and AENS. The RIs are calculated for all the scenarios mentioned above, which involve the integration of PEV charging stations and SPDGs. Table 7 contains customer information, while Table 8 presents statistical variables, including failure and repair rates, and average outage time for the IEEE 33-bus network. After implementing PEV charging stations, both consumer-oriented and load (energy)-oriented RIs show a decline. Conversely, the integration of SPDG units into the DN improves both types of RIs. This improvement is attributed to the ability of SPDG units to efficiently manage bus voltage, which enhances power transfer capability and minimizes power loss by regulating supplied power to the system. Moreover, SPDG units directly influence power flow by controlling injected power. The variation of RIs for different CSs is portrayed in Fig. 18. Table 9 demonstrates that the reliability indices deteriorate following the installation of PEV charging stations. The value of SAIFI is 0.1008 failures/customer in a year in CS1, i.e., before the allocation of PEV charging stations and SPDG units. When two PEV charging stations are optimally allocated at buses 20 and 4, the SAIFI is raised to 0.1768 failures/customer in a year which is 75.3 % more than the base value. The value of SAIDI and CAIDI also rose to a higher value than their base value. Likewise, the allocation of PEV charging stations has a detrimental impact on the energy-oriented RIs, such as EENS and AENS. Integrating PEVCS into the DN leads to a rise in the energy not supplied to meet the load demand, resulting in a rise in the associated indices. This increment in RIs is unfavorable for the distribution system. Distributing two charging station loads between two nodes results in higher reliability compared to concentrating both charging stations at a single node. When strong nodes of the electric power grid and high-traffic-density nodes of the transport network merge, the connecting paths can become congested. Therefore, distributing charging stations offers the additional advantage of providing charging capability to a larger number of electric vehicles traveling on various routes, reducing traffic congestion on specific paths leading to the concentrated charging loads. Hence, introducing a certain quantity of energy into the distribution network is favorable to enhance its reliability. One feasible approach is to utilize SPDG units, which inject active and reactive power based on the system's needs. Optimally integrating multiple SPDG units into the network improves the system's reliability. After integrating SPDG units, all reliability indices are studied, and their impact is presented in Table 9. It must be noted that in CS3 when two SPDG units are positioned optimally at bus 12 and 31, the value of SAIFI, SAIDI, and CAIDI decreased which is advantageous from the standpoint of reliability. The value of these indices decreased by 1.1%, 0.8 %, and 0.2 % as compared to CS2. Similarly, EENS and AENS are improved by 3.2 % and 4.2 %, respectively, in comparison to CS2 where two PEV charging stations were allocated only. In CS4, two PEV charging stations and two SPDG units are allocated in the distribution system which leads to further deterioration of the reliability indicators due to the heavy additional load of PEVs. Consequently, the integration of DGs leads to a continuous reduction in these reliability indices. With the addition of more DGs to the system, both the duration of disturbances and the frequency of interruptions in the network decrease. This decrease in disturbances and interruptions results in lower SAIDI and SAIFI values. Hence, achieving a decrease in SAIDI and SAIFI values is essential for enhancing the reliability of the DN. It is important to highlight that both EENS and AENS increase with an increasing number of SPDGs. For instance, when there are only two SPDGs, the AENS value is 15.4395 kWh per customer per year, but this increases to 15.9876 kWh per customer per annum when an additional SPDG is added to the network. As more SPDGs are integrated, it leads to an increase in the indices for energy not supplied. This minimization in EENS and AENS values is beneficial for a reliable power network, demonstrating an improvement in the electric network's reliability with the integration of SPDGs and sufficient reliability data. Further, case studies have been performed to increase the number of PEV charging stations and SPDG individually and simultaneously. It is realized that as the number of PEV loads rises, the reliability indices deteriorate. On the other hand, the reliability of the network increases by raising the number of SPDG units.

Table 7. Customer data at different load points

Number of load points	Load points	Number of customers
1	2	26
7	3, 18, 19, 20, 21, 22, 23	23
3	4, 14, 29	31
11	5, 6, 12, 13, 15, 16, 17, 26, 27, 28, 33	16
2	7, 8	52
2	9, 10	15
2	24, 25	109
1	11	12
1	30	25
1	31	39
1	32	35

Table 8. Statistical parameters at load points

Load Point	Failure rate (Failure per year)	Load Point	Outage duration (Hour per year)
19	0.02	5, 6	0.02
5, 6, 8, 9,11, 12, 14 to 17, 26 to 28, 33	0.03	2, 3, 4	0.03
3, 18 to 23	0.04	11	0.1
1	0.05	9, 10,12 to 15, 16 to 23, 26 to 28	0.2
4, 13	0.06	14, 29	0.3
31	0.07	31	0.4
7, 30	0.09	30	0.5
32	0.1	7, 8, 32	0.6
24, 25	0.19	24, 25	1.1
29	0.54		

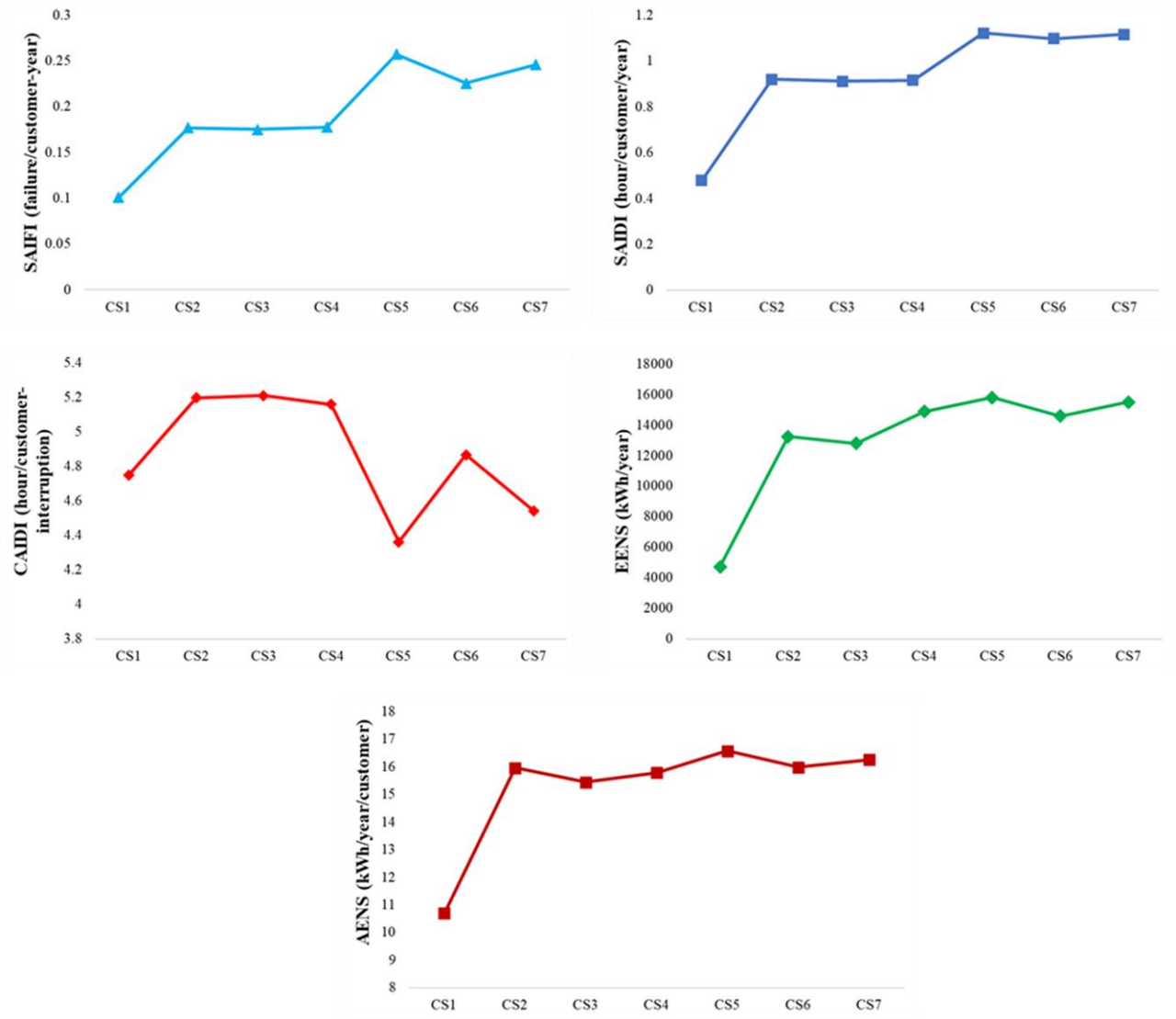

Fig. 18. Variation of different reliability indices in accordance with load change

Table 9. Reliability parameters for different case studies in IEEE 33-bus system

Case-studies	SAIFI	SAIDI	CAIDI	EENS	AENS
CS1	0.1008	0.4785	4.7474	4719.65	10.69319
CS2	0.1768	0.9189	5.197398	13228.92	15.9576
CS3	0.17494	0.9113	5.209215	12799.4	15.4395
CS4	0.17751	0.9157	5.158583	14876.5	15.7874
CS5	0.2571	1.1212	4.360949	15781.5	16.574
CS6	0.2254	1.0971	4.867347	14571.8	15.9876
CS7	0.2456	1.1156	4.542345	15487.6	16.2516

7. Conclusion

This study introduces a novel methodology for the optimal deployment of PEVCSs within the IEEE 33-bus system framework, incorporating solar-powered distributed generation (SPDG) units to address the increased energy demand.

The primary focus was minimizing active power loss, improving voltage regulation, and enhancing the VSI within distribution networks (DNs). The proposed approach utilized two-loss sensitivity factors (LSFs) to rank load buses based on their criticality, which proved effective in identifying optimal locations for PEVCSs. Through rigorous analysis and multiple case studies, the key findings of the study are as follows:

1. Reduction in Active Power Loss: The integration of PEVCSs and SPDG units significantly reduced active power loss. Specifically, the active power loss decreased from 202.67 kW in the baseline scenario to 24.59 kW in the best-case scenario, representing an 87.86% reduction. This substantial decrease underscores the effectiveness of the proposed optimization model.

2. Voltage Profile Improvement: The deployment of SPDG units alongside PEVCSs contributed to improved voltage profiles across the network. The minimum voltage magnitude observed at bus-18 increased from 0.9131 per unit (p.u.) to 0.9915 p.u. post-integration, indicating an improved voltage profile.

3. Voltage Stability Index (VSI): The lowest VSI value recorded improved from 0.6827 p.u. to 0.8798 p.u. in the optimal deployment scenario, highlighting the positive impact on network stability and the reduced risk of voltage collapse.

4. Reliability Indices: The integration strategy also positively affected the reliability indices of the DN. Increasing the number of SPDG units enhances network reliability by introducing redundancy and resilience, ensuring continuous power supply even if some units fail. This decentralized generation reduces the strain on central power plants, minimizes transmission losses, and improves the network's ability to manage demand fluctuations. Additionally, SPDG units can provide backup power during outages and integrate seamlessly with smart grids for real-time monitoring and adaptive management.

5. Practical Implications: The practical implications of this study are profound. By optimizing the placement of PEVCSs and integrating renewable energy sources, DNs can enhance their efficiency, sustainability, and reliability. This approach supports the broader goals of environmental sustainability and energy security, providing a robust framework for the large-scale deployment of PEV infrastructure powered by renewable energy sources.

6. Future Research Directions: Future research could further explore the dynamic interactions between PEVCSs and other renewable energy sources under varying operational conditions. Additionally, investigating the economic impacts and cost-benefit analysis of such integrations would provide a comprehensive understanding of the feasibility and long-term benefits of the proposed methodology. Expanding the applicability of this approach to diverse geographic and climatic settings could also offer valuable insights for global energy transformation strategies.

These numerical outcomes and detailed insights demonstrate the robustness of the proposed model and its potential for practical application in real-world scenarios. The statistically significant improvements in power loss reduction, voltage stability, and RIs provide strong validation for the proposed methodology. The results offer valuable guidance for policymakers and industry stakeholders in the strategic planning and deployment of PEV infrastructure, contributing to the development of sustainable and resilient power distribution systems.

References

1. Jing R, Wang X, Zhao Y, et al (2021) Planning urban energy systems adapting to extreme weather. Advances in Applied Energy 3:100053. https://doi.org/10.1016/j.adapen.2021.100053

2. Griffin PW, Hammond GP, McKenna RC (2021) Industrial energy use and decarbonisation in the glass sector: A UK perspective. Advances in Applied Energy 3:100037. https://doi.org/10.1016/j.adapen.2021.100037

3. Turan MT, Ates Y, Erdinc O, et al (2019) Effect of electric vehicle parking lots equipped with roof mounted photovoltaic panels on the distribution network. International Journal of Electrical Power & Energy Systems 109:283–289. https://doi.org/10.1016/j.ijepes.2019.02.014

4. Muthukumar K, Jayalalitha S (2016) OC. International Journal of Electrical Power & Energy Systems 78:299–319. https://doi.org/10.1016/j.ijepes.2015.11.019

5. Gökçek T, Turan MT, Ateş Y, Arabul AY (2022) A bi-level charging management approach for electric truck charging stationconsidering power losses. Turkish J Electr Eng Comput Sci 30:943–960. https://doi.org/10.55730/1300-0632.3820

6. I. Szuvovivski, T.S.P. Fernandes, A.R. Aoki Simultaneous allocation of capacitors and voltage regulators at distribution networks using Genetic Algorithms and Optimal Power Flow. Int J Electr Power Energy Syst 40:62–69

7. Hien NC, Mithulananthan N, Bansal RC (2013) Location and Sizing of Distributed Generation Units for Loadabilty Enhancement in Primary Feeder. IEEE Systems Journal 7:797–806. https://doi.org/10.1109/JSYST.2012.2234396

8. Bilal M, Rizwan M (2021) Integration of electric vehicle charging stations and capacitors in distribution systems with vehicle-to-grid facility. Energy Sources, Part A: Recovery, Utilization, and Environmental Effects 1–30. https://doi.org/10.1080/15567036.2021.1923870

9. Ahmad F, Ashraf I, Iqbal A, et al (2022) A novel AI approach for optimal deployment of EV fast charging station and reliability analysis with solar based DGs in distribution network. Energy Reports 8:11646–11660. https://doi.org/10.1016/j.egyr.2022.09.058

10. Moradi MH, Zeinalzadeh A, Mohammadi Y, Abedini M (2014) An efficient hybrid method for solving the optimal sitting and sizing problem of DG and shunt capacitor banks simultaneously based on imperialist competitive algorithm and genetic algorithm. International Journal of Electrical Power & Energy Systems 54:101–111. https://doi.org/10.1016/j.ijepes.2013.06.023

11. Zeinalzadeh A, Mohammadi Y, Moradi MH (2015) Optimal multi objective placement and sizing of multiple DGs and shunt capacitor banks simultaneously considering load uncertainty via MOPSO approach. International Journal of Electrical Power & Energy Systems 67:336–349. https://doi.org/10.1016/j.ijepes.2014.12.010

12. Quadri IA, Bhowmick S, Joshi D (2018) A comprehensive technique for optimal allocation of distributed energy resources in radial distribution systems. Applied Energy 211:1245–1260. https://doi.org/10.1016/j.apenergy.2017.11.108

13. Rastgou A, Moshtagh J, Bahramara S (2018) Improved harmony search algorithm for electrical distribution network expansion planning in the presence of distributed generators. Energy 151:178–202. https://doi.org/10.1016/j.energy.2018.03.030

14. Kumar S, Mandal KK, Chakraborty N (2019) Optimal DG placement by multi-objective opposition based chaotic differential evolution for techno-economic analysis. Applied Soft Computing 78:70–83. https://doi.org/10.1016/j.asoc.2019.02.013

15. Gampa SR, Das D (2015) Optimum placement and sizing of DGs considering average hourly variations of load. International Journal of Electrical Power & Energy Systems 66:25–40. https://doi.org/10.1016/j.ijepes.2014.10.047

16. Ismael SM, Abdel Aleem SHE, Abdelaziz AY, Zobaa AF (2018) Optimal Conductor Selection of Radial Distribution Feeders: An Overview and New Application Using Grasshopper Optimization Algorithm. In: Classical and Recent Aspects of Power System Optimization. Elsevier, pp 185–217

17. Islam MR, Lu H, Hossain MJ, Li L (2019) Mitigating unbalance using distributed network reconfiguration techniques in distributed power generation grids with services for electric vehicles: A review. Journal of Cleaner Production 239:117932. https://doi.org/10.1016/j.jclepro.2019.117932

18. Ma T-Y, Xie S (2021) Optimal fast charging station locations for electric ridesharing with vehicle-charging station assignment. Transportation Research Part D: Transport and Environment 90:102682. https://doi.org/10.1016/j.trd.2020.102682

19. Rahmani-andebili M, Venayagamoorthy GK (2015) SmartPark placement and operation for improving system reliability and market participation. Electric Power Systems Research 123:21–30. https://doi.org/10.1016/j.epsr.2015.01.016

20. Bilal M, Rizwan M (2020) Electric vehicles in a smart grid: a comprehensive survey on optimal location of charging station. IET Smart Grid 3:267–279. https://doi.org/10.1049/iet-stg.2019.0220

21. El-Zonkoly A, dos Santos Coelho L (2015) Optimal allocation, sizing of PHEV parking lots in distribution system. International Journal of Electrical Power & Energy Systems 67:472–477. https://doi.org/10.1016/j.ijepes.2014.12.026

22. Tolabi HB, Ara AL, Hosseini R (2020) A new thief and police algorithm and its application in simultaneous reconfiguration with optimal allocation of capacitor and distributed generation units. Energy 203:117911. https://doi.org/10.1016/j.energy.2020.117911

23. Lin X, Sun J, Ai S, et al (2014) Distribution network planning integrating charging stations of electric vehicle with V2G. International Journal of Electrical Power & Energy Systems 63:507–512. https://doi.org/10.1016/j.ijepes.2014.06.043

24. Wang C, Dunn R, Robinson F, et al (2017) Active–reactive power approaches for optimal placement of charge stations in power systems. International Journal of Electrical Power & Energy Systems 84:87–98. https://doi.org/10.1016/j.ijepes.2016.04.047

25. Xu H, Miao S, Zhang C, Shi D (2013) Optimal placement of charging infrastructures for large-scale integration of pure electric vehicles into grid. International Journal of Electrical Power & Energy Systems 53:159–165. https://doi.org/10.1016/j.ijepes.2013.04.022

26. Dong X, Mu Y, Xu X, et al (2018) A charging pricing strategy of electric vehicle fast charging stations for the voltage control of electricity distribution networks. Applied Energy 225:857–868. https://doi.org/10.1016/j.apenergy.2018.05.042

27. Wang Y, Shi J, Wang R, et al (2018) Siting and sizing of fast charging stations in highway network with budget constraint. Applied Energy 228:1255–1271. https://doi.org/10.1016/j.apenergy.2018.07.025

28. Qu Z, Xu C, Yang F, et al (2023) Market clearing price-based energy management of grid-connected renewable energy hubs including flexible sources according to thermal, hydrogen, and compressed air storage systems. Journal of Energy Storage 69:107981. https://doi.org/10.1016/j.est.2023.107981

29. Nie X, Mansouri SA, Jordehi AR, Tostado-Véliz M (2024) A two-stage optimal mechanism for managing energy and ancillary services markets in renewable-based transmission and distribution networks by participating electric vehicle and demand response aggregators. International Journal of Electrical Power & Energy Systems 158:109917. https://doi.org/10.1016/j.ijepes.2024.109917

30. Ahmad F, Iqbal A, Ashraf I, et al (2022) Optimal location of electric vehicle charging station and its impact on distribution network: A review. Energy Reports 8:2314–2333. https://doi.org/10.1016/j.egyr.2022.01.180

31. Bilal M, Rizwan M (2021) Intelligent Algorithm based Efficient Planning of Electric Vehicle Charging Station: A Case Study of Metropolitan City of India. Scientia Iranica 0–0. https://doi.org/10.24200/sci.2021.57433.5238

32. Awasthi A, Venkitusamy K, Padmanaban S, et al (2017) Optimal planning of electric vehicle charging station at the distribution system using hybrid optimization algorithm. Energy 133:70–78. https://doi.org/10.1016/j.energy.2017.05.094

33. Pazouki S, Mohsenzadeh A, Ardalan S, Haghifam M-R (2015) Simultaneous Planning of PEV Charging Stations and DGs Considering Financial, Technical,and Environmental Effects. Canadian Journal of Electrical and Computer Engineering 38:238–245. https://doi.org/10.1109/CJECE.2015.2436811

34. Zhang X, Yu X, Ye X, Pirouzi S (2023) Economic energy management of networked flexi-renewable energy hubs according to uncertainty modeling by the unscented transformation method. Energy 278:128054. https://doi.org/10.1016/j.energy.2023.128054

35. Jordehi AR, Mansouri SA, Tostado-Véliz M, et al (2024) Industrial energy hubs with electric, thermal and hydrogen demands for resilience enhancement of mobile storage-integrated power systems. International Journal of Hydrogen Energy 50:77–91. https://doi.org/10.1016/j.ijhydene.2023.07.205

36. Ahmad F, Khalid M, Panigrahi BK (2021) An enhanced approach to optimally place the solar powered electric vehicle charging station in distribution network. Journal of Energy Storage 42:103090. https://doi.org/10.1016/j.est.2021.103090

37. Qian K, Zhou C, Allan M, Yuan Y (2011) Modeling of Load Demand Due to EV Battery Charging in Distribution Systems. IEEE Transactions on Power Systems 26:802–810. https://doi.org/10.1109/TPWRS.2010.2057456

38. Pieltain Fernandez L, Gomez San Roman T, Cossent R, et al (2011) Assessment of the Impact of Plug-in Electric Vehicles on Distribution Networks. IEEE Transactions on Power Systems 26:206–213. https://doi.org/10.1109/TPWRS.2010.2049133

39. Wang X, Karki R (2017) Exploiting PHEV to Augment Power System Reliability. IEEE Transactions on Smart Grid 8:2100–2108. https://doi.org/10.1109/TSG.2016.2515989

40. Božič D, Pantoš M (2015) Impact of electric-drive vehicles on power system reliability. Energy 83:511–520. https://doi.org/10.1016/j.energy.2015.02.055

41. Khalafian F, Iliaee N, Diakina E, et al (2024) Capabilities of compressed air energy storage in the economic design of renewable off-grid system to supply electricity and heat costumers and smart

charging-based electric vehicles. Journal of Energy Storage 78:109888. https://doi.org/10.1016/j.est.2023.109888

42. Kumar A, Meena NK, Singh AR, et al (2019) Strategic integration of battery energy storage systems with the provision of distributed ancillary services in active distribution systems. Applied Energy 253:113503. https://doi.org/10.1016/j.apenergy.2019.113503

43. Chen C, Duan S (2014) Optimal Integration of Plug-In Hybrid Electric Vehicles in Microgrids. IEEE Transactions on Industrial Informatics 10:1917–1926. https://doi.org/10.1109/TII.2014.2322822

44. de Quevedo PM, Munoz-Delgado G, Contreras J (2019) Impact of Electric Vehicles on the Expansion Planning of Distribution Systems Considering Renewable Energy, Storage, and Charging Stations. IEEE Transactions on Smart Grid 10:794–804. https://doi.org/10.1109/TSG.2017.2752303

45. Bukar AL, Tan CW, Lau KY (2019) Optimal sizing of an autonomous photovoltaic/wind/battery/diesel generator microgrid using grasshopper optimization algorithm. Solar Energy 188:685–696. https://doi.org/10.1016/j.solener.2019.06.050

46. Zhou X, Mansouri SA, Jordehi AR, et al (2023) A three-stage mechanism for flexibility-oriented energy management of renewable-based community microgrids with high penetration of smart homes and electric vehicles. Sustainable Cities and Society 99:104946. https://doi.org/10.1016/j.scs.2023.104946

47. Kabir MN, Mishra Y, Ledwich G, et al (2014) Improving voltage profile of residential distribution systems using rooftop PVs and Battery Energy Storage systems. Applied Energy 134:290–300. https://doi.org/10.1016/j.apenergy.2014.08.042

48. Shariful Islam M, Mithulananthan N, Quoc Hung D (2019) Coordinated EV charging for correlated EV and grid loads and PV output using a novel, correlated, probabilistic model. International Journal of Electrical Power & Energy Systems 104:335–348. https://doi.org/10.1016/j.ijepes.2018.07.002

49. Ahmadian A, Sedghi M, Aliakbar-Golkar M, et al (2016) Optimal probabilistic based storage planning in tap-changer equipped distribution network including PEVs, capacitor banks and WDGs: A case study for Iran. Energy 112:984–997. https://doi.org/10.1016/j.energy.2016.06.132

50. Mansouri SA, Javadi MS, Ahmarinejad A, et al (2021) A coordinated energy management framework for industrial, residential and commercial energy hubs considering demand response programs. Sustainable Energy Technologies and Assessments 47:101376. https://doi.org/10.1016/j.seta.2021.101376

51. Mansouri SA, Ahmarinejad A, Javadi MS, et al (2021) Chapter 9 - Demand response role for enhancing the flexibility of local energy systems. In: Graditi G, Somma MD (eds) Distributed Energy Resources in Local Integrated Energy Systems. Elsevier, pp 279–313

52. Norouzi M, Aghaei J, Pirouzi S, et al (2022) Flexibility pricing of integrated unit of electric spring and EVs parking in microgrids. Energy 239:122080. https://doi.org/10.1016/j.energy.2021.122080

53. Bilal M, Rizwan M, Alsaidan I, Almasoudi FM (2021) AI-Based Approach for Optimal Placement of EVCS and DG With Reliability Analysis. IEEE Access 9:154204–154224. https://doi.org/10.1109/ACCESS.2021.3125135

54. Ahmad F, Bilal M (2023) Allocation of plug-in electric vehicle charging station with integrated solar powered distributed generation using an adaptive particle swarm optimization. Electrical Engineering. https://doi.org/10.1007/s00202-023-02087-9

55. Bamisile O, Obiora S, Huang Q, et al (2020) Towards a sustainable and cleaner environment in China: Dynamic analysis of vehicle-to-grid, batteries and hydro storage for optimal RE integration. Sustainable Energy Technologies and Assessments 42:100872. https://doi.org/10.1016/j.seta.2020.100872

56. Kamran M, Raugei M, Hutchinson A (2021) A dynamic material flow analysis of lithium-ion battery metals for electric vehicles and grid storage in the UK: Assessing the impact of shared mobility and end-of-life strategies. Resources, Conservation and Recycling 167:105412. https://doi.org/10.1016/j.resconrec.2021.105412

57. Pal A, Bhattacharya A, Chakraborty AK (2021) Placement of Public Fast-Charging Station and Solar Distributed Generation with Battery Energy Storage in Distribution Network Considering Uncertainties and Traffic Congestion. Journal of Energy Storage 41:102939. https://doi.org/10.1016/j.est.2021.102939

58. Fathy A, Abdelaziz AY (2020) Competition over resource optimization algorithm for optimal allocating and sizing parking lots in radial distribution network. Journal of Cleaner Production 264:121397. https://doi.org/10.1016/j.jclepro.2020.121397

59. Saldanha JJA, Nied A, Trentini R, Kutzner R (2024) AI-based optimal allocation of BESS, EV charging station and DG in distribution network for losses reduction and peak load shaving. Electric Power Systems Research 234:110554. https://doi.org/10.1016/j.epsr.2024.110554

60. Rene EA, Tounsi Fokui WS, Nembou Kouonchie PK (2023) Optimal allocation of plug-in electric vehicle charging stations in the distribution network with distributed generation. Green Energy and Intelligent Transportation 2:100094. https://doi.org/10.1016/j.geits.2023.100094

61. Dharavat N, Sudabattula SK, Velamuri S, et al (2022) Optimal Allocation of Renewable Distributed Generators and Electric Vehicles in a Distribution System Using the Political Optimization Algorithm. Energies 15:6698. https://doi.org/10.3390/en15186698

62. Mohanty AK, Suresh Babu P, Salkuti SR (2022) Optimal Allocation of Fast Charging Station for Integrated Electric-Transportation System Using Multi-Objective Approach. Sustainability 14:14731. https://doi.org/10.3390/su142214731

63. Jamatia P, Bhattacharjee S, Sharma S (2022) Allocation of Electric Vehicle Charging Station in Distribution Network along with Distributed Generation Sources. In: 2022 IEEE 6th International Conference on Condition Assessment Techniques in Electrical Systems (CATCON). IEEE, pp 196–201

64. Deb S, Tammi K, Kalita K, Mahanta P (2018) Impact of Electric Vehicle Charging Station Load on Distribution Network. Energies 11:178. https://doi.org/10.3390/en11010178

65. Ahmad F, Alam MS, Shariff SM, Krishnamurthy M (2019) A Cost-Efficient Approach to EV Charging Station Integrated Community Microgrid: A Case Study of Indian Power Market. IEEE Transactions on Transportation Electrification 5:200–214. https://doi.org/10.1109/TTE.2019.2893766

66. Shiau C-SN, Peterson SB, Michalek JJ (2010) Optimal Plug-In Hybrid Vehicle Design and Allocation for Minimum Life Cycle Cost, Petroleum Consumption and Greenhouse Gas Emissions. In: Volume 4: 12th International Conference on Advanced Vehicle and Tire Technologies; 4th International Conference on Micro- and Nanosystems. ASMEDC, pp 183–195

67. Negarestani S, Fotuhi-Firuzabad M, Rastegar M, Rajabi-Ghahnavieh A (2016) Optimal Sizing of Storage System in a Fast Charging Station for Plug-in Hybrid Electric Vehicles. IEEE Transactions on Transportation Electrification 2:443–453. https://doi.org/10.1109/TTE.2016.2559165

68. Ahmad F, Iqbal A, Asharf I, Marzband M, Khan I (2023) Placement and Capacity of EV Charging Stations by Considering Uncertainties With Energy Management Strategies. IEEE Transactions on Industry Applications 59:3865–3874. https://doi.org/ 10.1109/TIA.2023.3253817

69. Nurmuhammed M, Akdağ O, Karadağ T (2023) A novel modified Archimedes optimization algorithm for optimal placement of electric vehicle charging stations in distribution networks. Alexandria Engineering Journal 84:81–92. https://doi.org/10.1016/j.aej.2023.10.055

70. Archana AN, Rajeev T (2021) A Novel Reliability Index Based Approach for EV Charging Station Allocation in Distribution System. IEEE Transactions on Industry Applications 57:6385–6394. https://doi.org/10.1109/TIA.2021.3109570

71. Zhao W, Wang L, Mirjalili S (2022) Artificial hummingbird algorithm: A new bio-inspired optimizer with its engineering applications. Computer Methods in Applied Mechanics and Engineering 388:114194. https://doi.org/10.1016/j.cma.2021.114194

72. Alsattar HA, Zaidan AA, Zaidan BB (2020) Novel meta-heuristic bald eagle search optimisation algorithm. Artificial Intelligence Review 53:2237–2264. https://doi.org/10.1007/s10462-019-09732-5

73. Mirjalili S, Gandomi AH, Mirjalili SZ, et al (2017) Salp Swarm Algorithm: A bio-inspired optimizer for engineering design problems. Advances in Engineering Software 114:163–191. https://doi.org/10.1016/j.advengsoft.2017.07.002

74. Qi X, Khattak BN, Alam A, et al (2023) Optimal energy modeling and planning in the power system via a hybrid firefly and cuckoo algorithm in the presence of renewable energy sources and electric vehicles. Alexandria Engineering Journal 76:333–348. https://doi.org/10.1016/j.aej.2023.06.036

Nomenclature

PEV	Plug-in electric vehicles	GWO	Grey wolf optimization
SPDG	Solar-powered distributed generation	GWOPSO	Hybrid Grey wolf optimizer particle swarm optimization
DER	Distributed energy resources	MOPSO	Multi-objective particle swarm optimization
DG	Distributed generation	TLBO	Teaching learning-based optimization
PEVCS	Plug-in electric vehicles charging station	GOA	Grasshopper optimization algorithm
GA	Genetic algorithm	SAIFI	System average interruption frequency index
PSO	Particle swarm optimization	SAIDI	System average interruption duration index

CAIDI	Customer average interruption duration index	AENS	Average energy not supplied
EENS	Expected Energy Not Supplied	AHA	Artificial hummingbird algorithm
BESA	Bald eagle search algorithm	SSA	Salp swarm algorithm
SOC	State of charge	LSF	Loss sensitivity factor
AVDI	Average voltage deviation index	VSI	Voltage stability index
RI	Reliability indicators	FF	Fill factor
FS	Food source	TF	Territorial foraging
ESS	Energy storage system	PS	Power system

Abbreviations

DM_{avg}	Average driven miles between two interval points	ρ_{ti}	Driving probability
SOC_{min}	Minimum state of charge	I_{SC}	Short circuit current of the Solar PV panel
SOC_{max}	Maximum state of charge	V_{OC}	Open circuit voltage of the Solar PV panel
t_A	Arrival time	V_{SI}	Voltage at specific solar irradiance
t_D	Departure time	V_{TC}	Temperature coefficient of voltage
PEV_{CR}	Charging rate	T_{cell}	Temperature of the solar cell
Δt	Time duration	I_{SI}	Current produced at specific solar irradiance
AER_{PEV}	All electric range of PEV	SI_{avg}	Average value of solar irradiance
P_{dem}^{PEV}	Total EV demand	I_{TC}	Temperature coefficient of current
N	Number of EVs that can be charged	$T_{ambient}$	Ambient temperature
$SI(t)$	Solar irradiance at each time instant	$T_{nominal}$	Nominal temperature
$P_{Solar\ PV}$	Power output of solar PV	α_{SI}, β_{SI}	Shape parameters of the beta function
$N_{Solar\ PV}$	Number of solar panels	$P_{eff/b}$	Total effective active power loads beyond the node b
V_{max}	Maximum voltage	PEV_{DCR}	Discharging rate
I_{max}	Maximum current	δ_{base}	Failure rate
$Q_{eff/b}$	Total effective reactive power loads beyond the node q	T_{base}	Duration of outage
V_b	Voltage of the bus q	ΔP_{PEV}	Integrated active power load
$P_{l,k}$	Active power loss of the k^{th} line	C_i	Number of customers connected to the ith bus
$Q_{l,k}$	Reactive power loss of the k^{th} line	P_{loss}^{base}	Base case active power loss
R_k	Resistance of the k^{th} line	P_{gi}	Active power generation of i^{th} bus
X_k	Reactance of the k^{th} line	Q_{gi}	Reactive power generation of i^{th}
M	Number of buses	P_{di}	Active power demand of i^{th}
V_m	System's nominal voltage	Q_{di}	Reactive power demand of i^{th}
V_i	Voltage at i^{th} bus	η_{CR}^{PEV}	Charging efficiency

P_{base}	Base values of active power demand	PEV_{CR}	Charging rate
SOC_{max}^{PEV}	Maximum possible state of charge of the PEV battery		